Atmospheric Research 278 (2022) 106345

Contents lists available at ScienceDirect

Atmospheric Research

journal homepage: www.elsevier.com/locate/atmosres

Simulation of the effects of biomass burning in a mesoscale convective system in the central amazon

Flávio A.F. D'Oliveira [a], Julia C.P. Cohen [a,b], Dominick V. Spracklen [c], Adan S.S. Medeiros [d], Glauber G. Cirino [a,b], Paulo Artaxo [e], Cleo Q. Dias-Júnior [a,d,f,*]

[a] Postgraduate Program on Environmental Sciences – PPGCA, Federal University of Pará (UFPA), Belém, PA, Brazil
[b] Faculty of Meteorology, Federal University of Pará (UFPA), Belém, PA, Brazil
[c] School of Earth and Environment, University of Leeds, Leeds, United Kingdom
[d] Postgraduate Program in Climate and Environment (CLIAMB, INPA/UEA), Manaus, AM, Brazil
[e] Institute of Physics, University of Sao Paulo: Sao Paulo, SP, Brazil
[f] Department of Physics, Federal Institute of Pará (IFPA), Belém, PA, Brazil

ARTICLE INFO

Keywords:
Biomass burning
Downdrafts
Convective Systems
Amazonia

ABSTRACT

During the dry season of 2014, the formation of a mesoscale convective system (MCS) caused intense precipitation and strong winds in the central Amazon region. In this period, cases of MCS that occurred during the days when there were higher concentrations of CO were analyzed. Through this criterion, a case of MCS occurred on August 16th, 2014 was selected. We used the chemical-atmospheric model WRF-Chem to assess the influence of biomass burning aerosol on the intensity of precipitation, winds, vertical and horizontal transport associated with this convective system. We show that biomass burning aerosol reduces the strength of the mesoscale convective system, with less vertical and horizontal transport of carbon monoxide and ozone. In the absence of biomass burning aerosol downdrafts and precipitation rate are more intense, and cloud development up to 5 km is more developed, making the horizontal flow and vertical transport of ozone more intense, however, much more efficient in reducing the concentrations of other gases.

1. Introduction

The main contributors to the emission of aerosols in the Brazilian Amazon region are the biomass burning (BB), from deforestation and agricultural practices (Echalar et al., 1998; Martin et al., 2010; Reddington et al., 2015). The emission of BB aerosol in the Amazon atmosphere has many impacts on weather and climate through feedback with radiation and clouds (Ramanathan et al., 2001; Kaufman and Koren, 2006; Rosenfeld et al., 2008). Particles between 0.1 and 2 μm in diameter absorb visible light more strongly and transform electromagnetic energy into thermal energy, reducing incident solar energy reaching the surface (Charlson et al., 1992; Ackerman et al., 2000; Schwartz and Buseck, 2000).

Aerosol particles, including BB aerosol, can also act as cloud condensation nuclei (CCN) and ice nuclei (Roberts et al., 2001; Spracklen et al., 2011), and may also alter the reflectivity of the cloud (Albrecht, 1989; Jiang and Feingold, 2006). BB aerosol can also alter the onset of precipitation. For example, Andreae et al. (2004) observed that dense smoke from Amazon forest fires, rich in BB, reduced the size of cloud droplets and delayed the onset of precipitation in the region. It is known that delays in the onset of precipitation can increase the lifetime of clouds, allowing the strengthening of air updrafts and downdrafts and consequently increasing cloud cover (Albrecht, 1989; Koren et al., 2004). Furthermore, we know that in the Amazon region the organization of clouds often takes the form of mesoscale convective systems (MCS), which are responsible for a significant amount of precipitation in the region (Houze, 2004). Rehbein et al. (2017) carried out a study on the climatology of MCS in the Amazon for 14 years (2000 to 2013) and showed that these systems occur frequently, including during the dry season in central Amazonia, which occurs between August and December (Marengo et al., 2001). It is also known that during the presence of MCS, the occurrence of downdrafts is common, which play an important role in the dynamics of gas transport in the Amazonia (Betts, 2002; Gerken et al., 2016; Dias-Júnior et al., 2017; Melo et al., 2019; Bezerra et al., 2021). Betts (2002) confirmed the increase in the concentration of ozone (O_3) at the surface in the Amazon, generated by

* Corresponding author at: Department of Physics, Federal Institute of Pará (IFPA), Belém, PA, Brazil.
E-mail address: cleo.quaresma@ifpa.edu.br (C.Q. Dias-Júnior).

https://doi.org/10.1016/j.atmosres.2022.106345
Received 15 April 2022; Received in revised form 29 June 2022; Accepted 14 July 2022
Available online 22 July 2022

the action of downdrafts, which, in addition to bringing cooler and drier air from higher layers of the atmosphere, also transport considerable amounts of O_3 to the surface.

During the rainy season in Amazonia, aerosol concentrations in the atmosphere are low and the characteristics of clouds formed in this environment resemble those observed in remote marine regions (Roberts et al., 2001; Williams, 2002; Martin et al., 2010). With data obtained during the Cooperative LBA Airborne Regional Experiment (LBA-Claire) campaign in the Amazon, Roberts et al. (2001) found mean CCN values of 267 cm^{-3}, typical values for maritme regions. Furthermore, the structure of clouds during the Amazon rainy season resembles those of oceanic areas, which is why the region is called a"green ocean" (Williams, 2002). Similar results were also found during the GoAmazon experiment (Martin et al., 2016; Giangrande et al., 2017; Machado et al., 2018). The GoAmazon experiment was a project that aimed to investigate the impacts of urban emissions from the city of Manaus, which is a major source of pollution located in the central Amazon and which is surrounded by a large area of tropical forest. The experiment collected data during the year 2014 to 2015 on the distribution of pollutants, such as aerosols and gases, as well as meteorological data (detailed information can be found in Martin et al. (2016)).

In contrast to the low concentrations of CCN observed for the rainy season, during the dry season concentrations can exceed 10,000 cm^{-3}, especially due to the greater number of fires at this time of year (Roberts, 2003; Rissler et al., 2004; Vestin et al., 2007). In addition, the rate of deforestation and fires has shown an increasing trend in recent years in the Amazon region (Barlow et al., 2019; Junior et al., 2020), promoting an increase in BB aerosol emissions and aerosol concentrations (Butt et al., 2021) with consequent changes in weather and climate of the Amazon.

Several studies have already been carried out in order to better understand the role of BB aerosols in cloud formation and consequently in precipitation rates (Chate et al., 2003; Andreae and Rosenfeld, 2008; Tao et al., 2012). However, there is no consensus in the literature regarding this role. Several authors suggest that"warm rain" processes (precipitation from shallow clouds, without ice content) would be suppressed under polluted conditions (large amounts of BB in the atmosphere) (Albrecht, 1989; Ramanathan et al., 2001; Rosenfeld, 1999). Furthermore, Wu et al. (2011) showed that BB aerosols in South America tend to reduce precipitation in the long term. A result similar to that shown in the work by Camponogara et al. (2014) where they observed that in environments with large amounts of aerosol there was an inhibition of precipitation associated with MCS in the Rio de la Plata basin. However, other works such as those by Lin et al. (2006) showed that the increase in aerosol optical depth (AOD) during the dry season in Amazonia was associated with increased precipitation and cloud cover in the years 2000 and 2003. Results by Koren et al. (2008) showed that aerosols can increase or decrease the cloud fraction and height depending on microphysics or aerosol absorption results, with the initial cloud fraction having an important role to determine on the balance between the two effects. Martins et al. (2009), using the BRAMS model, show that on polluted days the total precipitation can increase or decrease, depending on the level of pollution used as a reference. Also, according to Martins et al. (2009) the highest precipitation rates were found for the most polluted scenarios. Gonçalves et al. (2015) also investigated the relationship between aerosol concentration and precipitation rates in the Amazon region. They noted that the impact was dependent on atmospheric stability, with BB aerosol reducing precipitaion in more stable atmospheres whilst increasing precipitation in unstable atmospheres. Kolusu et al. (2015) used the UK Met Office Unified Model to suggest that BB aerosol resulted in an overall reduction in precipitation across the Amazon, with fewer but more intense rainfall events.

A regional model that has been widely used in recent years for a better understanding of the effects of aerosols on cloud formation, precipitation and atmosphere chemistry is the WRF (Weather Research and Forecasting) model (Grell et al., 2005) developed by collaborative participation between NCAR (National Center for Atmospheric Research), NOAA (National Oceanic and Atmospheric Administration) and others. This model has been frequently updated by several collaborators (WRF Release Information) and has also been coupled to a chemical model, where the effects of gases and aerosols aggregated with the atmosphere (WRF-Chem) can be observed for different regions of the planet (Borge et al., 2008; Conibear et al., 2018; Silver et al., 2020), and also for the Amazon region (Beck et al., 2013; Bela et al., 2015; Rafee et al., 2017; Butt et al., 2020; Liu et al., 2020). Archer-Nicholls et al. (2016) used WRF-Chem to show BB aerosol reduced convection and precipitation over the Amazon region. Liu et al. (2020) also used WRF-Chem to show BB aerosol reduces precipitation over the Amazon through both aerosol-radiation and aerosol-cloud interactions.

In this work we intend to contribute to a better understanding of the effects of BB concentrations on precipitation rates from MCS above Central amazon, similar to others studies already carried out. However, special attention will be given to the occurrence of downdrafts, arising from MCS, and the consequent transport of gases in the middle troposphere and close to the surface. For this, high resolution numerical simulations were performed with the WRF-Chem atmospheric model. This study has two objectives: 1) to verify if the MCS is enhanced or suppressed by the presence of aerosol from biomass burning emissions; 2) quantify the variation in the transport of gases such as O_3 and carbon monoxide (CO) in the event of a strengthened or suppressed storm. As far as we know, this is the first work that investigates the role of BB concentrations in the occurrence of downdrafts and in the transport of gases in the Amazon region.

2. Material and methods

2.1. Study area

The central Amazon region is largely covered by tropical forest and has several rivers, such as the Amazon, Negro and Solimões, in addition to topographical variations (Marinho et al., 2020). Moreover, the region is heavily influenced by local circulations, especially during the dry season (Dias et al., 2004; dos Santos et al., 2014), where these circulations have an influence on wind direction, temperature and precipitation patterns. Another feature of the region is that the Amazon basin is one of the continental regions with the cleanest air conditions (Williams, 2002), which makes it the perfect region to observe how changes in pollutant concentrations may have effects on MCS in the Amazon. The study area used in this work comprises the experimental sites: 1) Manacapurú, T3, (03° 12′ 49″ S, 60° 35′ 55″ W) 70 km from the city of Manaus (Dias-Júnior et al., 2017); 2) from the Cuieiras biological reserve, T0z, (02° 36′ 33″ S, 60° 12′ 33″ W), 60 km from Manaus (Araújo, 2002) and 3) (Fig. 1). These sites were implanted and instrumented during the Green Ocean Amazon experiment (GoAmazon2014/5) (Martin et al., 2016). It is important to mention that the T3 site is typically downwind of the city of Manaus, influenced by urban air masses (Trebs et al., 2012; Martin et al., 2016), while the T0z site is located north of the city of Manaus, which is not influenced by the transport of emissions from the city (Rizzo et al., 2013).

2.2. Data

The analyzes were centered during the dry season of central Amazon in the year 2014. During this period, cases of MCS that occurred during the days when there were higher concentrations of CO were analyzed. Through this criterion, a case of MCS occurred on August 16th, 2014 was selected. The motivation for this choice is due to the fact that this system had a great intensity of precipitation and associated wind speed through the experimental data, with the higher CO levels among the other MCSs that occurred in the period.

The experimental data from the T0z site used in this work were the air temperature measured at 50 m; the mixture ratio of CO and O_3

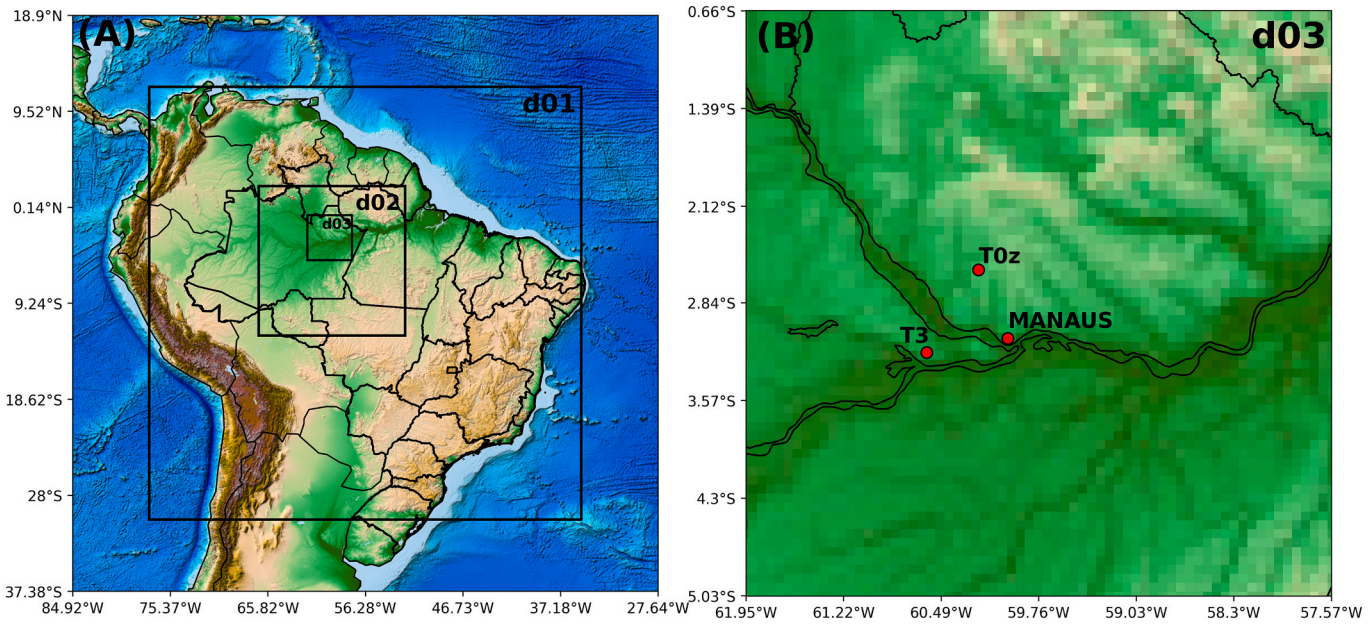

Fig. 1. The WRF-Chem domains used in the study in: (a) locations of the three domains; and (b) Domain d03 zoomed and the locations of surface stations are represented by red dots. (For interpretation of the references to colour in this figure legend, the reader is referred to the web version of this article.)

collected by gas analyzers (Picarro G2301 and 49i-TSi), where these sensors were installed in a micrometeorological tower and collected at a height of 39 m (Rizzo et al., 2013).

At site T3, temperature, precipitation and wind speed data were used, collected by the automatic weather station WXT520 (Vaisala), as well as data on the CO mixing ratio measured by Los Gatos ICOS N2O/CO-23D (LGR) and O_3 measured by the 49i TSi (Thermo) gas analyzer.

In the city of Manaus, SIPAM (Amazon Protection System) S-Band Radar data were additionally used. Satellite images were also used in the infrared channel (Band 4) of GOES-13 and data extracted from the reanalysis of the ERA5 model (Hersbach et al., 2020) of the ECMWF (European Center for Medium-Range Weather Forecasts). Radar and satellite data were used to identify the MCS that occurred in the central Amazon region in the dry period of 2014, and ERA5 data to identify the formation of this system.

2.3. Simulation descriptions

In this work, the WRF-Chem model in version 4.2 (Grell et al., 2005) was used to carry out the simulations shown here.

The following domains configurations, physical and chemistry options are shown in Table 1. In addition, an updated volatility baseline mechanism for secondary organic aerosol (SOA) formation was also included (Knote et al., 2015).

Initial and boundary conditions for chemistry and aerosols were taken from the Community Atmosphere Model with Chemistry (CAM-Chem) (Lamarque et al., 2012). For baseline and boundary weather conditions, data extracted from the ECMWF global reanalysis (Dee et al., 2011) were used with a time resolution of 6 h and 0.25 degrees of horizontal resolution.

Anthropogenic emissions data were extracted from the EDGAR-HTAP (Emissions Database for Global Atmospheric Research with Task Force on Hemispheric Transport of Air Pollution) version 2.2 database. These data are representative of the year 2010, which is the most recent dataset available, with a horizontal resolution of 0.1˚ x 0.1˚ (Janssens-Maenhout et al., 2019). Due to little information on anthropogenic emissions in the Amazon, some authors have used their own local emission inventories to better represent the chemistry in the central Amazon region (Rafee et al., 2017; Medeiros et al., 2017). Therefore, in this work, road transport and electricity emissions from the EDGAR-HTAP were modified according to local emission estimates, using the VEIN (Vehicle Emissions Inventory) model version 0.9.13 (Ibarra-Espinosa et al., 2018). VEIN is a bottom-up model used to obtain high resolution vehicle emissions inventories. The thermoelectric emissions, the type of fuel and its monthly consumption were provided by the Brazilian power plant (ELETROBR S, 2014). Gas emissions were entered in the d03 domain of the simulations as"POW" for energy emissions and"TRA" for transport emissions.

Table 1
WRF-Chem processes and inputs.

Process/Inputs	WRF-Chem Options	Reference
Long wave radiation	RRTMG	Iacono et al. (2008)
Short wave radiation	RRTMG	Iacono et al. (2008)
Boundary layer	MYNN 2.5	Nakanishi and Niino (2009)
Cloud mirophysics	Morrison 2-Moment	Morrison et al. (2009)
Cumulus cloud	Off	
Land surface	NOAH Surface Model	Ek et al. (2003)
Points along x and y coordinates	176 × 176 for d01, 178 × 181 for d02 and 163 × 163 for d03	
Horizontal resolution	27 km for d01, 9 km for d02 and 3 km for d03	
Vertical layers	60	
Gas-phase mechanism	MOZART	Knote et al. (2014)
Aerosol chemistry and Microphysics	MOSAIC with 4 bins	Zaveri et al. (2008) and Hodzic and Knote (2014)
Photolysis	New TUV	Tie (2003)

The simulation integration period started at 00 UTC on August 15th and ended at 00 UTC on August 17th, 2014, totaling 48 h of integration, with the first 24 h being discarded (spin-up). For this study, two simulations were carried out with the following characteristics: (1) bb_on simulation, where the estimated biomass burning emissions for the fires identified during the simulation period will be used; (2) bb_off simulation, where emissions from biomass burning will not be used. The objective of these two scenarios is to evaluate the behavior of the MCS in an experiment with bb_on, where it behaves as a control experiment in which biomass burning emissions are taken into account, and with

bb_off that simulates what it would be like without emissions of fires during the period, and thus verify how the MCS behaves in relation to precipitation and transport of O_3 and CO gases.

For biomass burning emissions, the NCAR Fire Inventories (FINN) version 1.5 was used (Wiedinmyer et al., 2011). These data are composed of a daily estimate of a 1 km^2 grid based on the location and time of active fires detected by the product of thermal and fire anomalies from the Moderate Resolution Imaging Spectroradiometer (MODIS) (Giglio et al., 2003). For each fire count, a burned area of 0.75 km^2 is assigned to grasslands and savannas, and 1 km^2 for other land cover. FINN data offers global coverage, high temporal and spatial resolution, and includes emissions for a large number of chemical species, including CO_2, CO, NOx, NH_3, CH_4 volatile and semi-volatile organic compounds (VOC and SVOC), black carbon (BC) and organic carbon (OC) aerosols. The FINN fire emissions are emitted in WRF-Chem using a diurnal cycle that peaks in the early afternoon (local-time) based on Giglio (2007) and then are injected evenly throughout the boundary layer (Dentener et al., 2006), as supported by analysis of plume heights over the Amazon (Marenco et al., 2016; Gonzalez-Alonso et al., 2019). FINN has been widely used in studies using atmospheric chemical transport models to simulate air quality changes from local to global scales. Fig. 2 shows the domains d02 (black square) and d03 (blue square) with all biomass burning emission points obtained through FINN data for the period August 15th, 2014 from 12 UTC to 12 UTC of the following day.

3. Results and discussion

3.1. Case study of a mesoscale convective system

The formation of this MCS occurred due to the confluence of winds caused by the gradient of temperature and specific humidity (Fig. 3). It is noted that in the North/Northeast region of the study area, the values of specific air temperature/humidity are lower/higher than the values observed in the South/Southeast region. For temperature, there is a gradient of 10°C, and for specific humidity, the gradient is 10 g kg^{-1}, and this gradient is the cause for the winds to converge in this region. East winds bring ocean humidity to the region and converge with westerly winds in the MCS formation region, favoring its formation.

The first convective cells of this MCS were observed at 07 UTC on August 16th, east of the city of Manaus. The evolution of this MCS can be seen in Fig. 4. At 09:15 UTC, the beginning of the formation of convective cell clusters can be observed (Fig. 4a). Around 12:15 UTC, the mature stage of the MCS can be seen, when the clouds were around the T0z site and the city of Manaus (Fig. 4b). The highest intensity of this MCS, as a function of the cloud top brightness temperature, occurred around 14:15 UTC, with cooler cloud tops near the T3 site (Fig. 4c) and at 18:45 UTC the MCS was already found further west of the sites (Fig. 4d). The dissipation of this MCS was observed at 03 UTC the following day, totaling a 'life cycle' of approximately 20 h, that is, a long life span according to the definition by Rehbein et al. (2019).

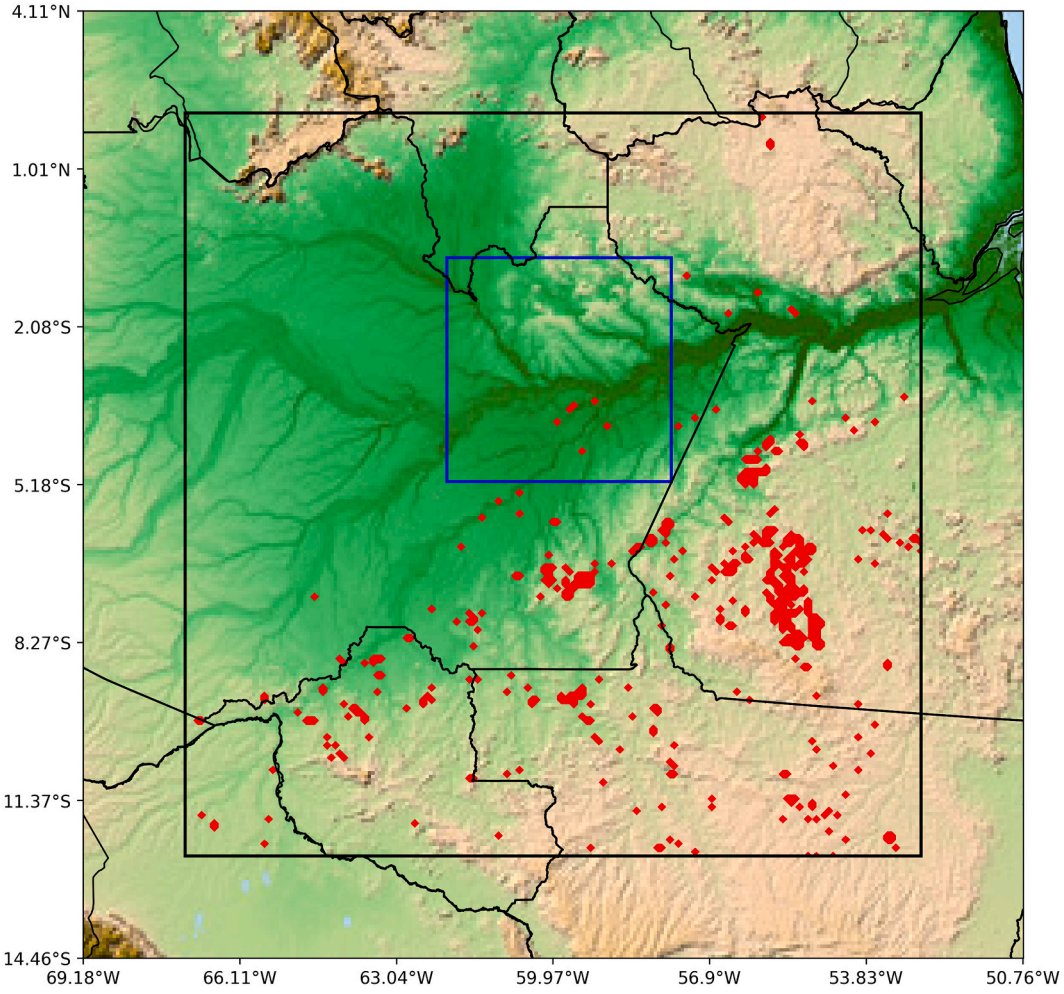

Fig. 2. FINN biomass burning emission points in domains d02 and d03 (highlighted by black and blue squares, respectively) in the 24-h period from 12 UTC on the 15th to 12 UTC on the 16th of August 2014. (For interpretation of the references to colour in this figure legend, the reader is referred to the web version of this article.)

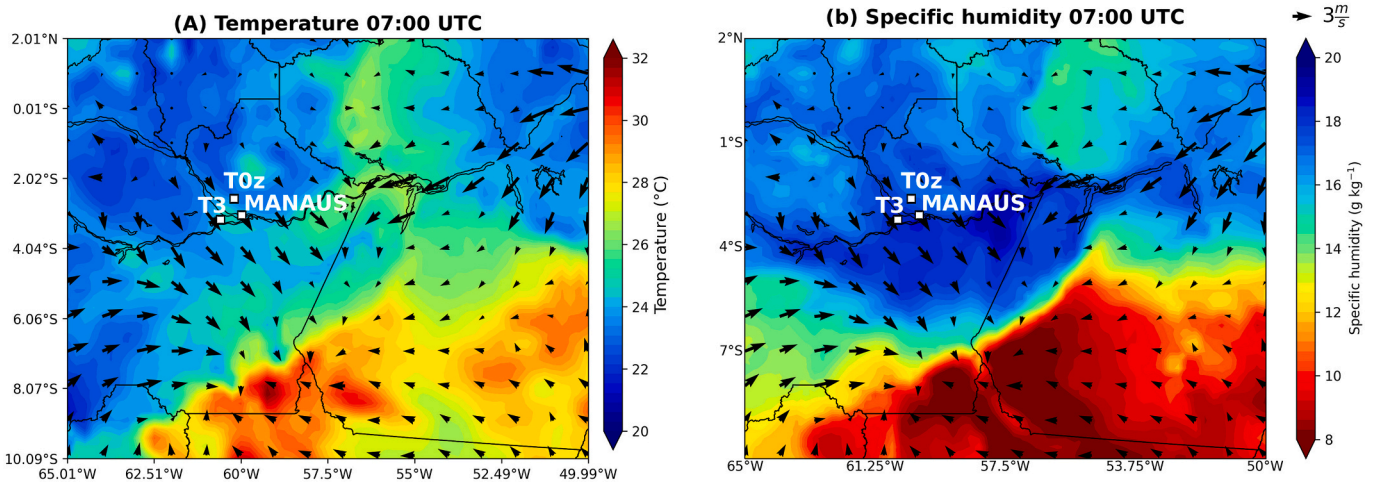

Fig. 3. Reanalysis data from the ERA5 model from 1000 hPa pressure level with a spatial resolution of 0.125° on August 16th, 2014 at 07 UTC: (A) Temperature (°C); and (B) Specific humidity (g kg^{-1}). The black arrows indicate the wind speed and direction and the yellow dots indicate the location of the experimental sites. (For interpretation of the references to colour in this figure legend, the reader is referred to the web version of this article.)

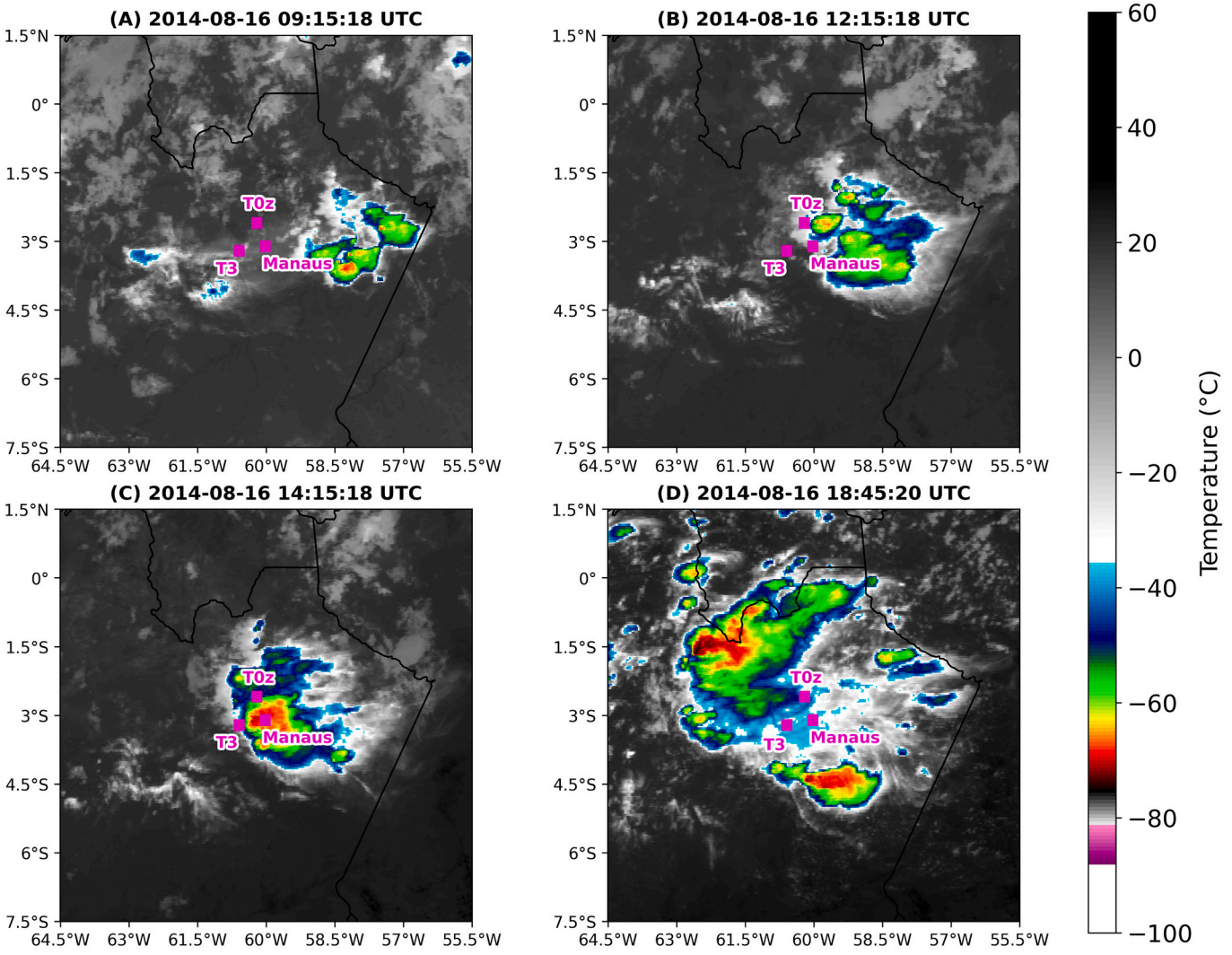

Fig. 4. Satellite images from GOES-13 on channel 4 (Infrared) for August 16, 2014: (a) 09:15 UTC; (b) 12:15 UTC; (c) 14:15 UTC; and (d) 18:45 UTC. Colors indicate cloud top temperature in Celsius degrees.

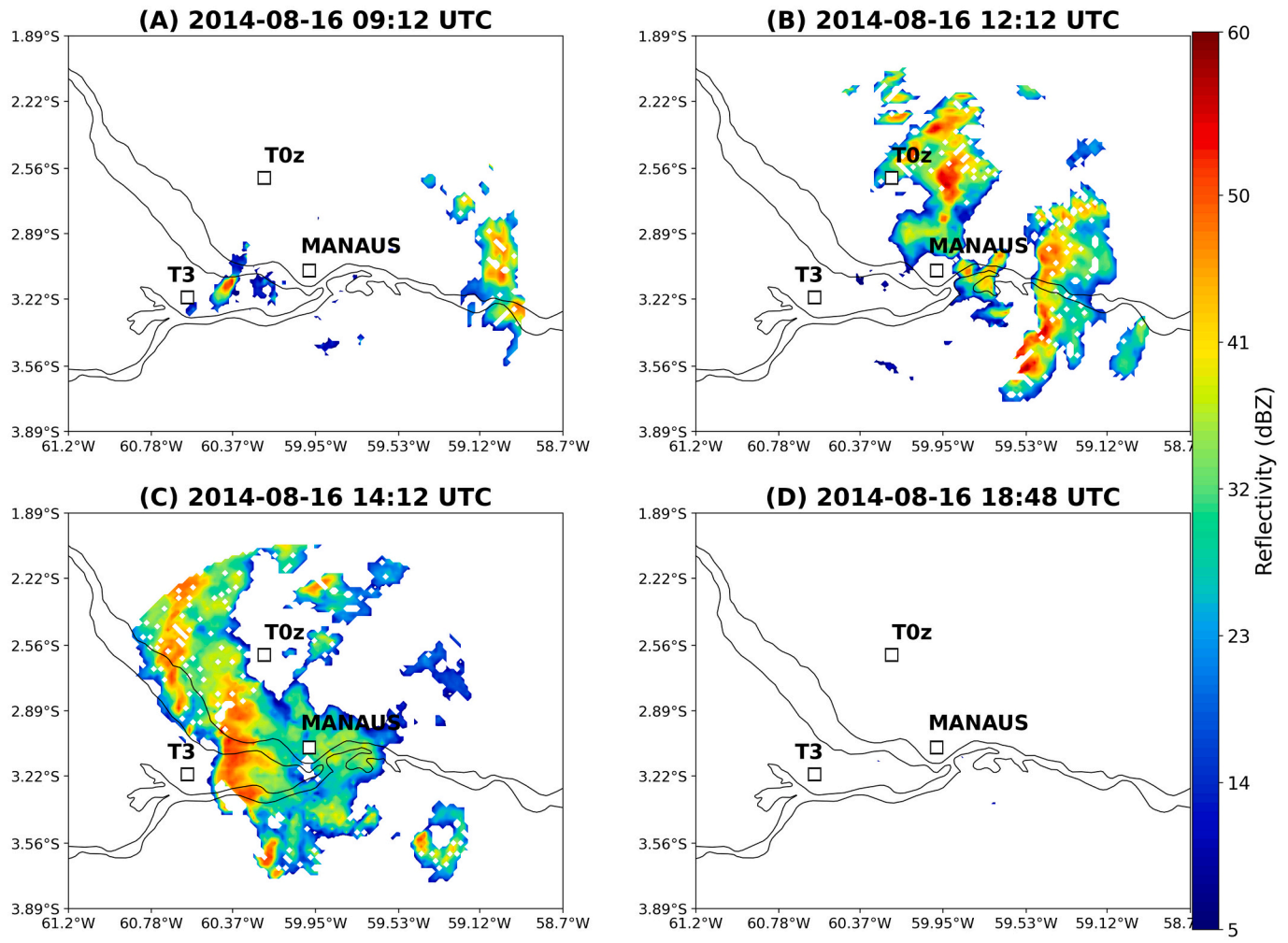

Fig. 5. CAPPI (Constant Altitude Plan Position Indicator) reflectivity of 1 km from Manaus SIPAM S-Band radar at: (a) 09:12 UTC; (b) 12:12 UTC; (c) 14:12; and (d) 18:48 UTC. The colors indicate the radar reflectivity in dBZ.

Fig. 5 shows the MCS through the reflectivity of SIPAM's S-Band radar in Manaus at times close to those shown in Fig. 4. At 09:12 UTC it is possible to observe the beginning of the formation of linear convective activity to the east of the sites. At 12:12 UTC, the MCS is already in the most mature stage on its way to the city of Manaus (Fig. 5b), and at 14:12 UTC it is closer to the T3 site (Fig. 5c). Finally, at 18:49 UTC the MCS is no longer visible in the radar region, corroborating with what was observed in Fig. 4.

3.2. *Passage of the MCS through the experimental sites*

Fig. 6 compares measured temperature against the bb_on and bb_off simulations. Note that around 13:10 and 14:40 UTC the measured temperature dropped rapidly at both T0z and T3 (reductions of 1.24 and 6.85 °C, respectively). These times correspond to situations in which these sites were covered by strong cloud cover (MCS), as shown in Figs. 4 and 5. The simulations reasonably reproduce the measured temperature at all locations, although there is a delay of 3 h compared to the measured data. In the bb_on scenario reductions of 6.55 and 7.02 °C (T3 and T0z, respectively) were simulated, while in the bb_off scenario the temperature drop was 8.73 and 7.72 °C (T3 and T0z, respectively). Note that there is greater cooling in the bb_off scenario (simulation without BB emissions) at the investigated sites.

Fig. 7 shows the precipitation rates and horizontal wind speed, obtained experimentally and through simulations at sites T0z (Fig. 7a-b) and T3 (Fig. 7c-d). There were no observed precipitation at site T0z, but in the simulation results the most intense precipitation was observed at 17 UTC in bb_on (0.53 mm hr^{-1}) and at 17:10 UTC in bb_off (7.08 mm hr^{-1}). At the T3 site, the most intense precipitation occurred at 14:30 UTC (37.96 mm hr^{-1}), while at bb_on it was observed at 18:10 UTC (4.1 mm hr^{-1}) and at bb_off also at 18:10 UTC (13.51 mm hr^{-1}). The accumulated precipitation was 0.13 and 1.90 mm (bb_on and bb_off respectively) for the T0z site, and 17.46, 1.81 and 4.19 mm (observed, bb_on and bb_off respectively) for the T3 site. The simulated precipitation rates, for the different scenarios, show that the precipitation intensity was lower than the observed values. It is worth noting that other studies that used the WRF-Chem for the region also observed underestimated precipitation in relation to measurements (Liu et al., 2020; Nascimento et al., 2021). In the simulations, precipitation intensity is lower in the bb_on simulation compared to the bb_off simulations (Fig. 7a-c).

Still in Fig. 7, it is possible to notice that the times of occurrence of precipitation were the same in which the presence of the MCS was observed in the different sites (Fig. 6). Furthermore, at these times observed horizontal wind speed increased substantially (Fig. 7b-d), to 5.07 m s^{-1} at 12:50 UTC at T0z, and 10.37 m s^{-1} at 14:20 UTC at T3. Typical wind speed at these sites is <2.5 m s^{-1} (Santana et al., 2018; Mendonça, 2021). Simulated horizontal wind speeds also increased substantially during the occurrence of precipitation, although simulated values overestimated in relation to measurements (Fig. 7 b-d). It is also noteworthy that during the presence of the MCS, the horizontal wind speed values are more intense in the bb_off scenario (13.54 and 18.33 m

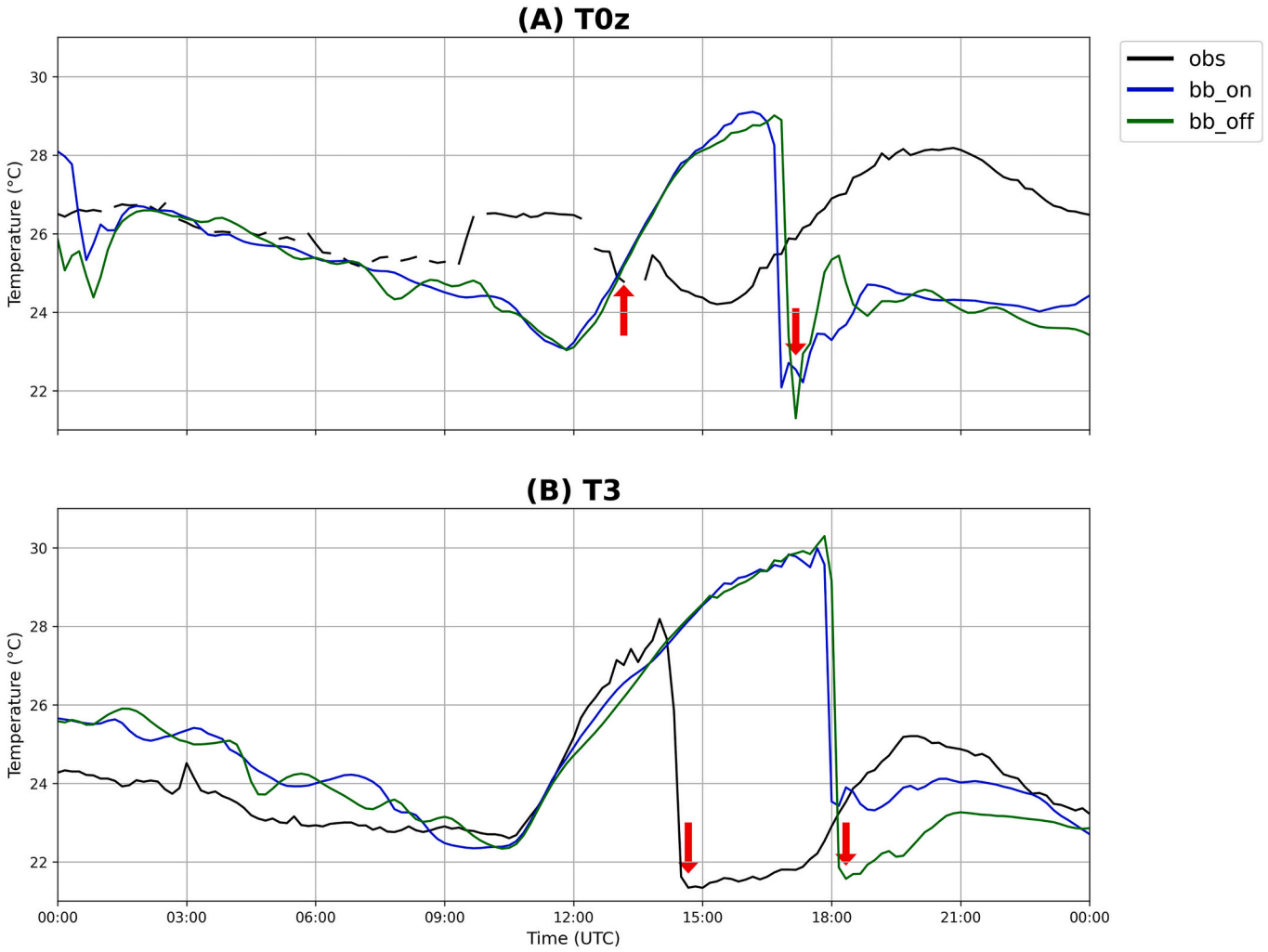

Fig. 6. Comparison of surface air temperature (°C) at (a) T0z; (b) T3 for measurements (black line), and simulated for bb_on scenario (blue line) and bb_off scenario (green line). (For interpretation of the references to colour in this figure legend, the reader is referred to the web version of this article.)

s^{-1} in T0z and T3, respectively) than in the bb_on scenario (9.24 and 16.85 m s^{-1} at T0z and T3, respectively). In a polluted scenario (bb_on) there are higher number of CCN, which causes the droplet growth to be impaired. In comparison, in the simulation without fires (bb_off), the cloud drops grow faster, as there is less CCN competing for humidity in the environment. Thus, the bb_off scenario can have larger droplets with faster growth, and as a consequence have more precipitation and more intense downdraft (cooling the surface more).

Fig. 8 compares observed and simulated concentrations of O_3 and CO at the measurement sites. In general, the simulations show that the concentrations of O_3 and CO increase and decrease, respectively, during the passage of the MCS in the two investigated sites, similar to that observed with the measurement data.

At the T0z site, the measured values show an increase in O_3 concentration of 14.99 ppbv and a reduction of CO of 32.06 ppbv between 12:00 and 15:20 UTC. In the bb_on simulation there was an increase in O_3 concentration of 2.44 ppbv and a reduction of CO of 14.28 ppbv between 16:00 and 16:50 UTC. In the bb_off simulation the O_3 increase was 4.62 ppbv and the CO reduction was 23.73 ppbv between 16:20 and 17:10 UTC.

At the T3 site, the measurement data showed that there was an increase in O_3 concentration of 31.9 ppbv and a reduction of CO of 90.33 ppbv between 13:50 and 14:30 UTC. In bb_on the O_3 increase was 8.82 ppbv and the CO reduction of 31.95 ppbv between 17:30 and 18:10 UTC, and in the bb_off the O_3 increase was 9.87 ppbv and the CO reduction of 42.12 ppvb between 17:00: 40 and 18:20 UTC.

Unfortunately, during the simulation period, it was not possible to compare the aerosol data from the modeling results with the AERONET measurements due to lack of data and the data coverage of MODIS was poor. It is important to note that in the bb_off simulations the increases in O_3 and the decreases in CO were greater than those simulated for the bb_on simulations for the two investigated sites.

The increase in surface O_3 concentrations during the passage of the MCS is due to the transport of O_3 from higher levels to the surface through the downdrafts, and as the bb_off scenario had higher values of wind associated with the MCS, it therefore transports a greater amount of O_3 to the surface. The reduction in CO concentration would be associated with a layer of air with low concentrations of CO, from higher levels, which is transported to the surface during the occurrence of downdrafts.

Several studies have already shown that downdrafts occur during the presence of MCS, which are responsible for altering the thermodynamics and chemistry in the middle and lower troposphere (Garstang et al., 1998; Betts, 2002; Gerken et al., 2016; Dias-Júnior et al., 2017; Melo et al., 2019; Bezerra et al., 2021, among others). These downdrafts are known to be very efficient in transporting cold, dry air from high altitudes towards the surface (Betts, 2002). In addition, pioneering works in the Amazon, such as those by Scala et al. (1990) and Garstang et al. (1998) already showed that these downdrafts bring with them a portion of air rich in O_3, and as a consequence the surface levels of this gas

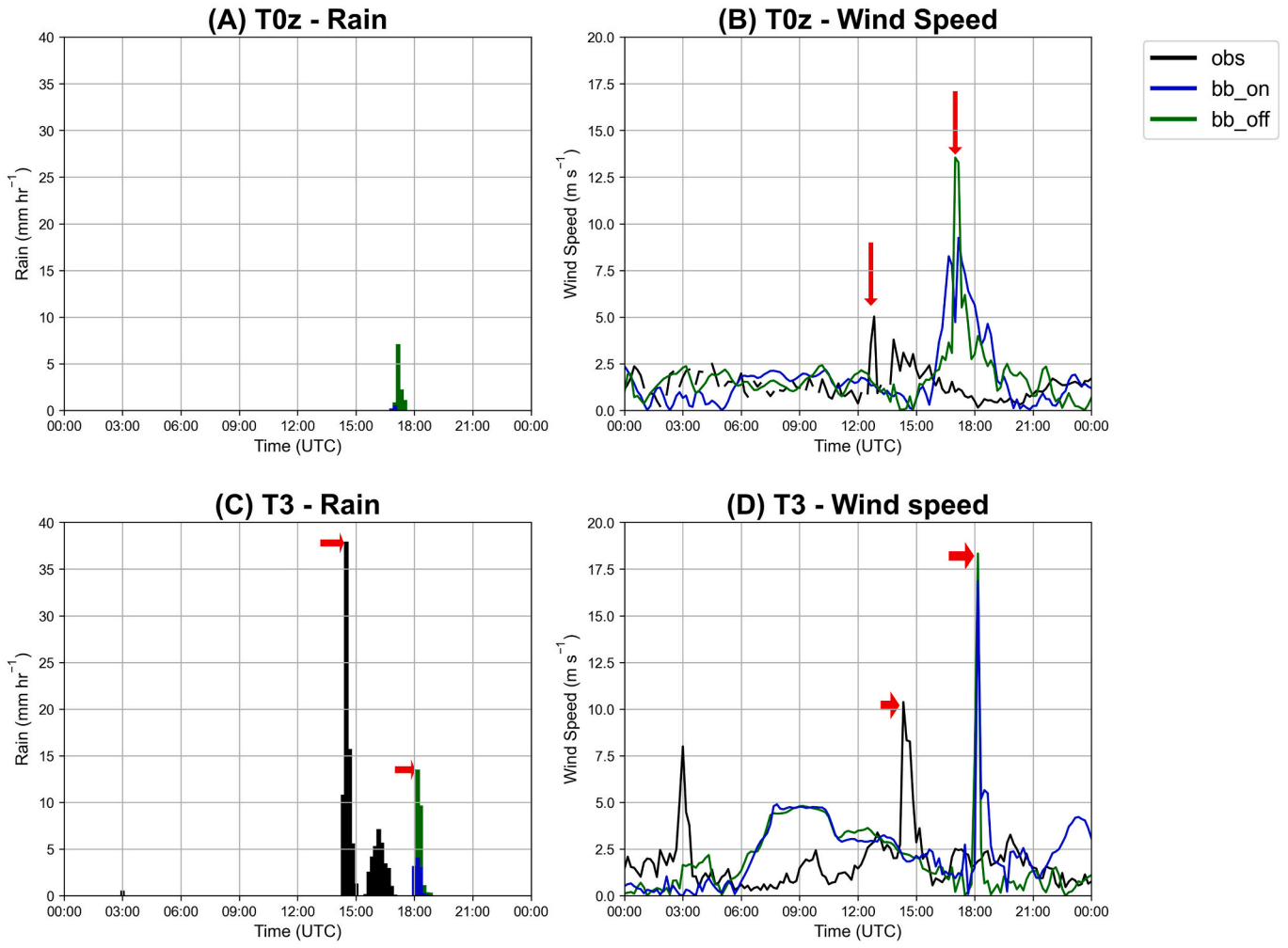

Fig. 7. Comparison of surface air temperature (°C) at (a) T0z; (b) T3 for measurements (black line), and simulated for bb_on scenario (blue line) and bb_off scenario (green line). (For interpretation of the references to colour in this figure legend, the reader is referred to the web version of this article.)

increase during the occurrence of these descending air movements. Other results that deserve attention were those shown in the work of Dias-Júnior et al. (2017) and Melo et al. (2019), where through experimental data and simulations with the BRAMS model, they showed that these downdrafts can generate low-level jets close to the surface and as a consequence O_3, CO and other gases can be transported tens of kilometers from the origin of the downdrafts. Recently, Bezerra et al. (2021) showed that a squall line produced downdrafts at different locations in the Amazon region, altering the chemistry and organization of atmospheric turbulence near the surface.

In the case study present here, it is possible to observe that the MCS produced strong downdrafts at the sites of T0z and T3, since at these sites there were sudden drops in temperature (Fig. 6a-b), an increase in horizontal wind speed (Fig. 7b-d) and rises/falls of O_3 /CO when precipitation occurred (Fig. 7a-c).

Another issue that deserves attention is related to the fact that in the bb_off simulation, the fingerprint of the downdraft were stronger than in the bb_on simulations, that is, it was in the bb_off simulation that the largest occurred: temperature drops, increases in horizontal wind speed and O_3 concentration, and decreases in CO concentration.

3.3. *Vertical transport of gases*

In this section, attention will be given to changes in the simulated vertical wind speed profiles and gas concentrations during the occurrence of downdrafts at site T3. The T3 site was chosen because the downdraft fingerprint were the strongest there, that is, it was where the greatest drops in temperature and CO concentrations occurred, and the greatest increases in O_3 concentration.

Fig. 9 shows the vertical section of the cloud water mixing ratio at the latitude of site T3 (−3.2133°), at 18:00 UTC in both scenarios. It is possible to notice that in the bb_off scenario there is a greater amount of cloud water up to 5 km, showing a more robust cloud development than in bb_on. In (A) the maximum value of the coud and ice mixing ratio is 1.34 g kg^{-1} while in bb_off this value is 3.3 g kg^{-1}. This indicates that in the bb_off simulation there is the presence of a more intense storm. These results reinforce the hypothesis raised that in the bb_off scenario, the lower concentration of CCN would be associated with larger drops and a greater amount of water to be precipitated.

In Fig. 10a-c the vertical profiles of the vertical wind speed (w) are shown. At 17:40 UTC (Fig. 10a), the moment before precipitation, the values of w were close to zero, especially in the layer of air between the ground and the height of 2000 m. At 18:10 UTC (Fig. 10b), approximate time of precipitation occurrence in the bb_off and bb_on simulations, it is observed that the values of the vertical wind component (w) were negative, indicating the occurrence of downdrafts. At the same time, at bb_off the speed of the most intense downdraft (−3.56 m s^{-1}) occurred at the level of 1750 m, while at bb_on at this same level the speed was −1.81 m s^{-1}. At 18:20 UTC (Fig. 10c), the moment immediately after the downdraft occurs, the values of w are again close to zero.

In Fig. 10d-f the vertical profiles of O_3 are shown. At 17:40 UTC (Fig. 10d) an O_3 -rich air plume located between 2 and 4 km is observed.

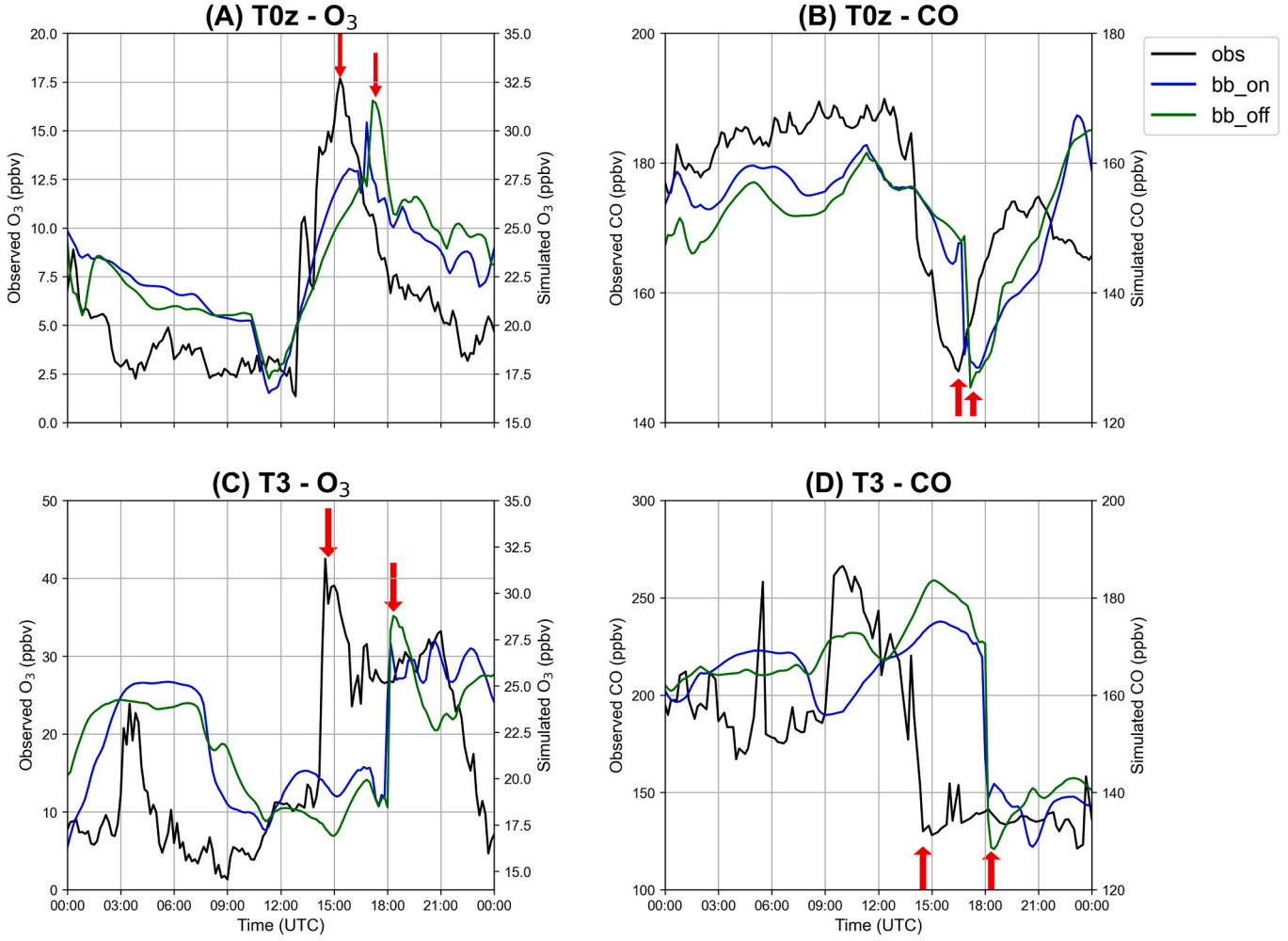

Fig. 8. Comparison of observed (black line) and simulated gas phase concentrations: O_3 concentrations at (A) T0z, (C) T3; CO concentrations at (B) T0z and (D) T3. Simulations are bb_on (blue line) and bb_off (green line) scenarios. (For interpretation of the references to colour in this figure legend, the reader is referred to the web version of this article.)

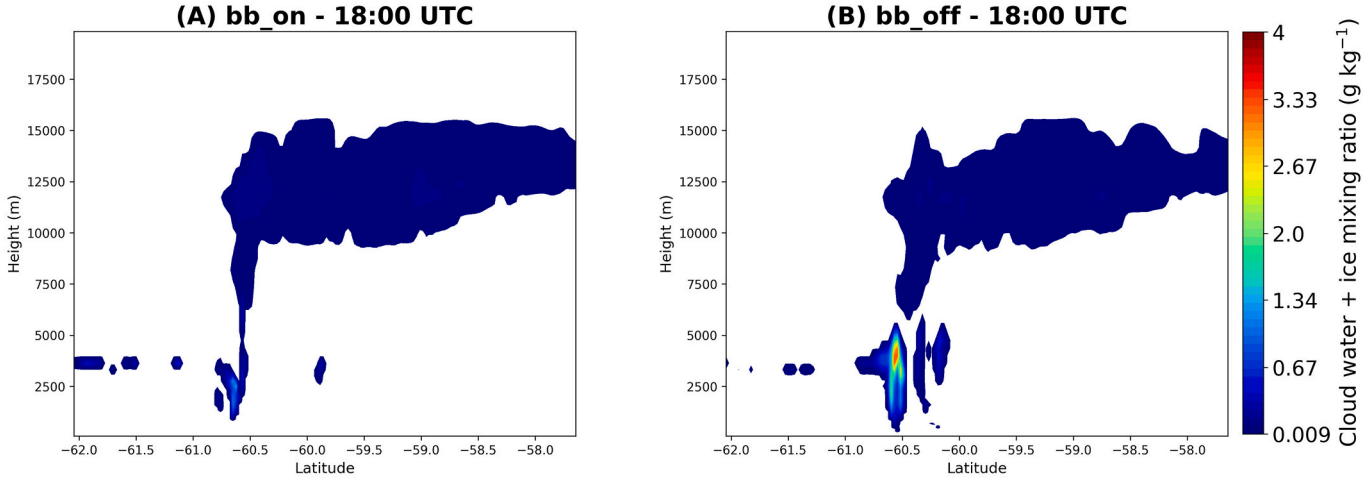

Fig. 9. Vertical section of the cloud water and ice mixing (g kg^{-1}) for the latitude of the T3 site (−3.2133°) at 18:00 UTC for the (A) bb_on and (B) bb_off simulations.

O_3 values in this region are around 35 ppbv in both scenarios, while on the surface O_3 concentrations are 18.89 and 19.12 ppbv (bb_on and bb_off, respectively). At 18:10 UTC (Fig. 10e), when the downdraft occurred, the presence of the O_3 -rich air plume between 2 and 4 km is no longer observed. At 18:20 UTC, after the downdraft occurs, it is noted that for the bb_off simulation there are practically no vertical gradients of O_3, while for the bb_on simulation there is a slight gradient between the surface and the level of 4 km. That is, in the bb_off simulation, the

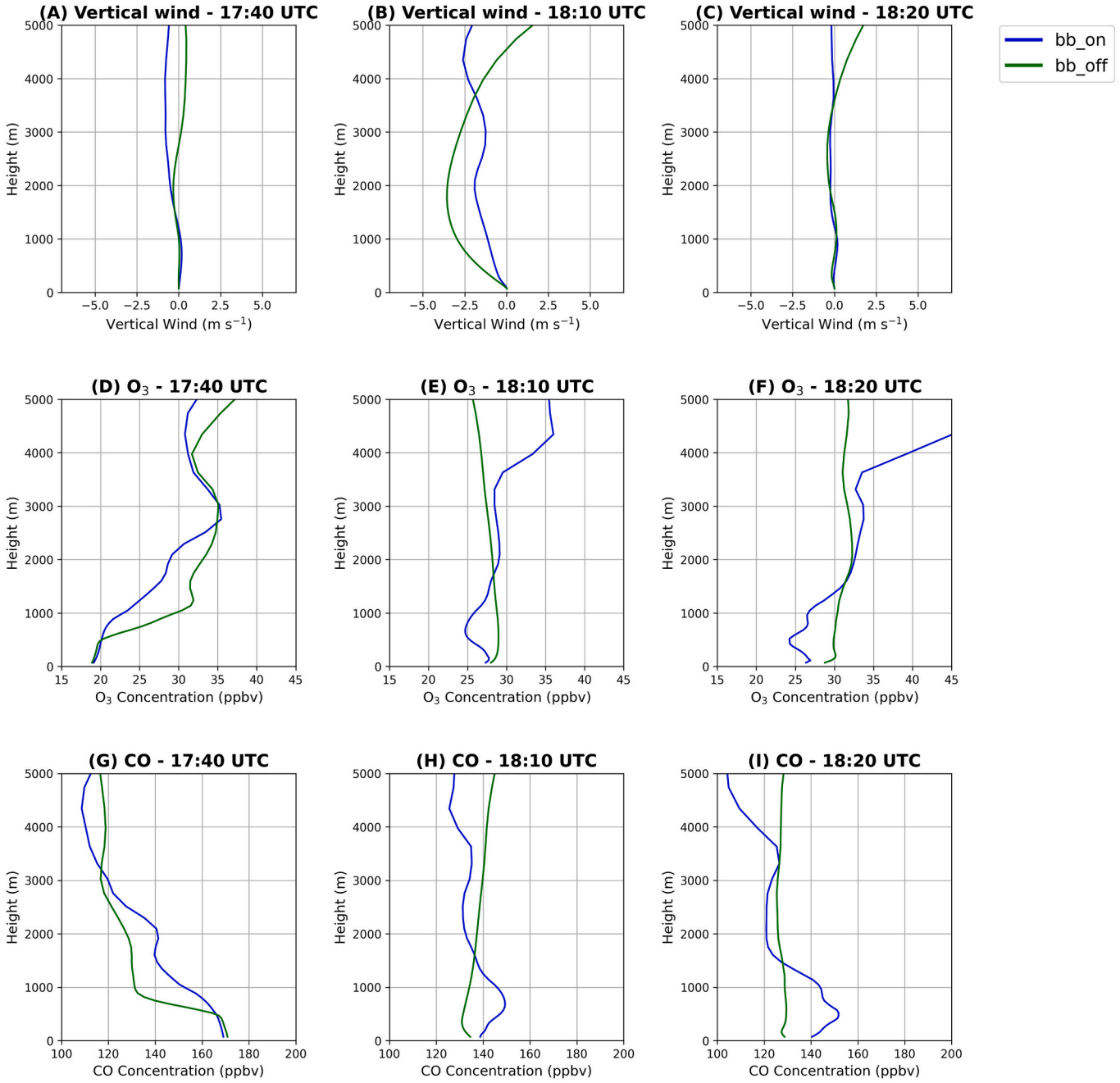

Fig. 10. Vertical profile in T3 for scenarios bb_on (blue line) and bb_off (green line) of vertical wind speed (w) at: (A) 17:40 UTC; (B) 18:10 UTC; and (C) 18:20 UTC. O_3 at: (D) 17:40 UTC; (E) 18:10 UTC; and (F) 18:20 UTC. CO at: (G) 17:40 UTC; (H) 18:10 UTC; and (I) 18:20 UTC. BC at: (J) 17:40 UTC; (K) 18:00 UTC; and (L) 18:20 UTC. (For interpretation of the references to colour in this figure legend, the reader is referred to the web version of this article.)

downdraft was more efficient in mixing O_3 throughout the layer.

Fig. 10g-i show the vertical CO profiles up to 5 km. At 17:40 UTC (Fig. 10g) previous to the downdraft, the concentration of CO is higher near the ground than at higher altitudes. The difference in CO concentration between the surface and the 3 km level was 49.4 and 53.71 ppbv for the bb_on and bb_off simulations, respectively. At 18:10 UTC (Fig. 10h) there is a marked reduction in CO concentrations on the surface (30.28 and 36.33 ppbv, in bb_on and bb_off, respectively), in both simulations, reinforcing the hypothesis that during the occurrence of the downdraft a layer of poorer CO air is carried down. At 18:20 UTC (Fig. 10i) it is observed that the vertical profile of CO in bb_off presents practically no gradients, similar to that observed for O_3.

3.4. Horizontal transport of gases during the presence of MCS

Fig. 11 presents the spatial distribution of the precipitation rate during the passage of the MCS in the d03 domain for the simulations with the different scenarios. The precipitation rate in both simulations showed the MCS propagating westward. However, the structure of the MCS was slightly different for the two scenarios. In its initial stage, at 15 UTC (Fig. 11a-b), the MCS was shown to be very similar for the two scenarios, and for the bb_on simulation, the convection organization is closer to a linear format. At 16:30 UTC (Figures 11bc-d), the MCS was over the city of Manaus in both simulations. At 18:10 UTC (Fig. 11e-f) it is observed that the MCS presented greater convective activity in its northern branch in both scenarios. At 19:30 UTC (Fig. 11g-h), the MCS

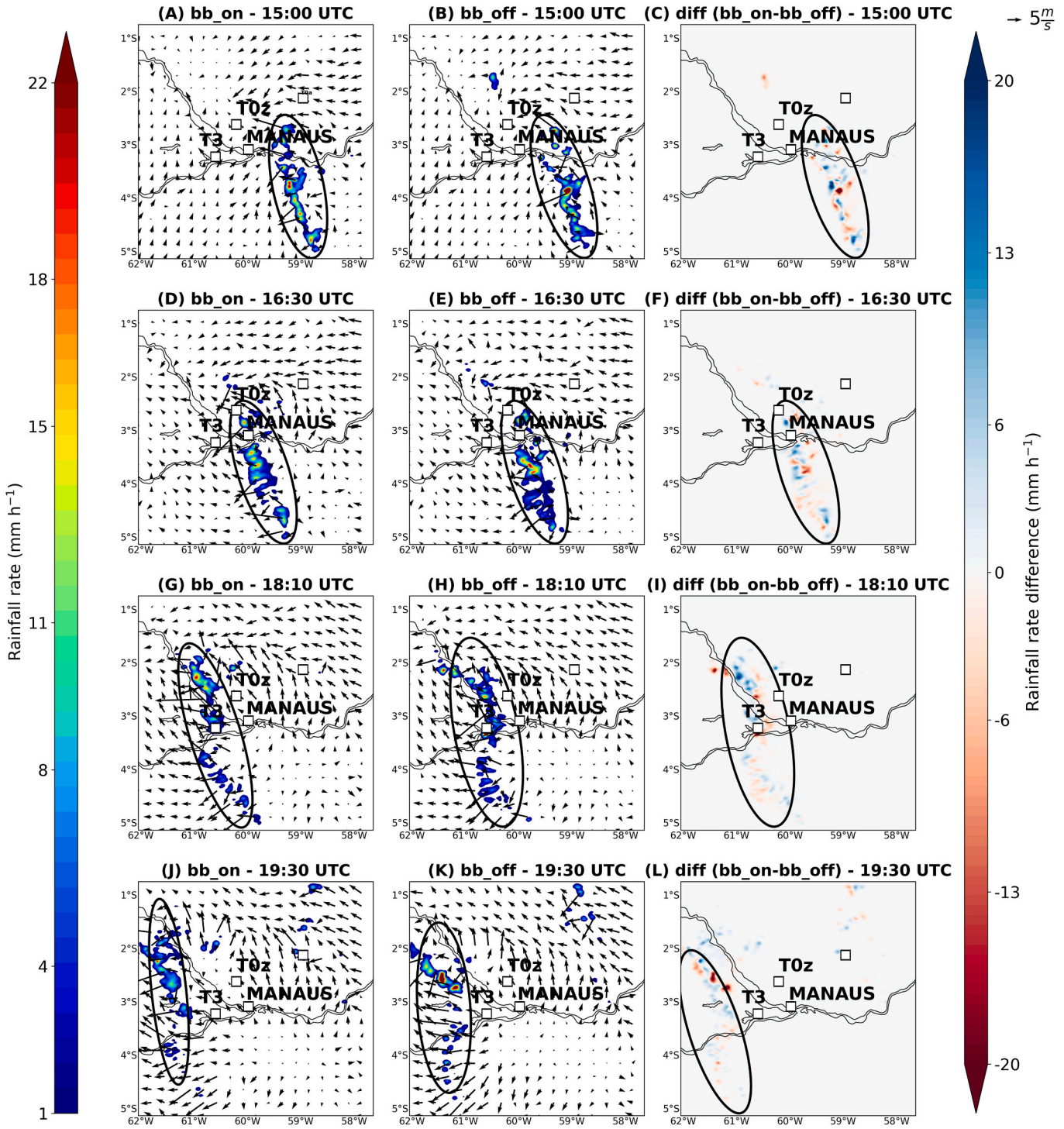

Fig. 11. Spatial distribution of precipitation rate or intensity (mm hr^{-1}) in the d03 domain: 15 UTC in (A) bb_on; (B) bb_off; and (C) diff; at 16:30 UTC on (D) bb_on; (E) bb_off; and (F) diff; at 18:10 UTC on (G)bb_on; (H) bb_off; and (I) diff; at 19:30 UTC on (J) bb_on; (K) bb_off; and (L) diff.

had already passed the T3 site in the simulations. Additionally, it is noted that the precipitation between the two scenarios is different, being more concentrated in the bb_off scenario than in bb_on.

Fig. 12 shows the spatial distribution of the surface concentration of O_3 in the d03 domain for the simulations with the bb_on and bb_off scenarios during the passage of the MCS. The black ellipses correspond to the positions of the MCS shown in Fig. 13. It is clearly noted that during the passage of the convective system the surface concentrations of O_3 increase, that is, as the system moves from East to West it causes elevations in the O_3 concentrations on its way. This increase is justified by the transport produced by the downdraft, in which O_3 is brought from the middle troposphere to the surface (Fig. 10). This result corroborates with the same results found in Melo et al. (2019).

Fig. 13 shows the spatial distribution of CO, similar to Fig. 12, during the passage of the MCS in the d03 domain. The black ellipses correspond to the positions of the MCS shown in Fig. 11. Clearly, a CO plume is observed coming from the southwest of the domain towards the MCS in both scenarios. The surface concentrations of CO present an opposite

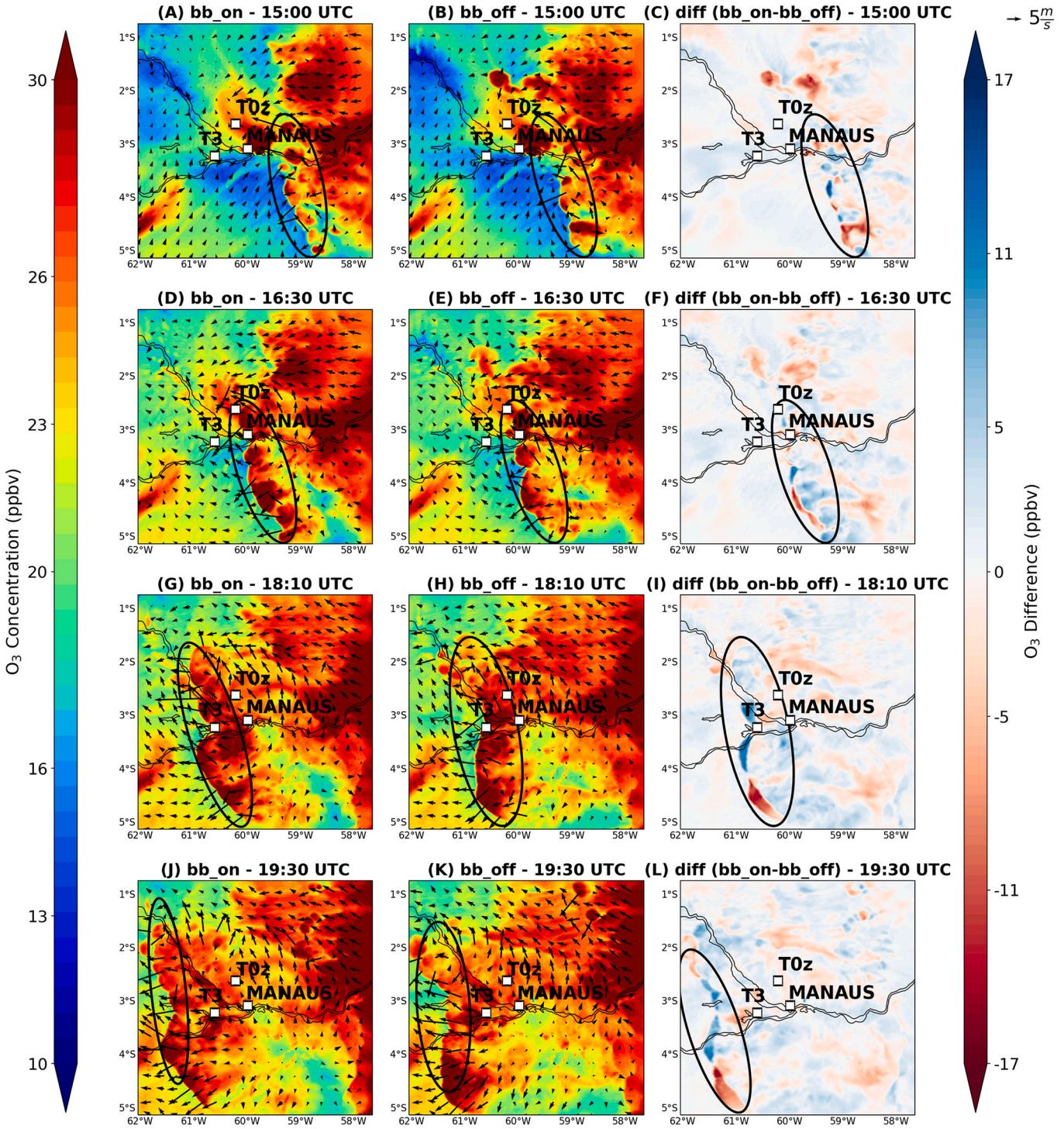

Fig. 12. Spatial distribution of surface-level O_3 concentration (ppbv) in the d03 domain at: 15 UTC on (A) bb_on; (B) bb_off; and (C) diff; at 16:30 UTC on (D) bb_on; (E) bb_off; and (F) diff; at 18:10 UTC on (G)bb_on; (H) bb_off; and (I) diff; at 19:30 UTC on (J) bb_on; (K) bb_off; and (L) diff.

behavior to that observed for O_3, that is, the passage of the MCS reduces the concentrations of CO along its path. Such behavior can be justified by the vertical transport produced by the downdraft, where air with low concentrations of CO is brought to the surface (Fig. 10).

Fig. 14 shows the average horizontal fluxes of O_3 and CO estimated from the simulations performed for the experimental site T3. For the calculation of such fluxes, the following procedure was carried out: the average values (equivalent to 24 h of simulation) of the horizontal wind speed (mU) and the concentrations of O_3 (mO_3) and CO (mCO) were calculated. Then the fluctuations of U, O_3 and CO were calculated through Eqs. (1), (2) and (3) respectively for every 10 min (output of the simulations). With the fluctuations it was possible to calculate the horizontal fluxes of O_3 (fhO_3) and CO (fhCO) by Eqs. (4) and (5).

$$fU = U - mU \tag{1}$$

$$fO_3 = O_3 - mO_3 \tag{2}$$

$$fCO = CO - mCO \tag{3}$$

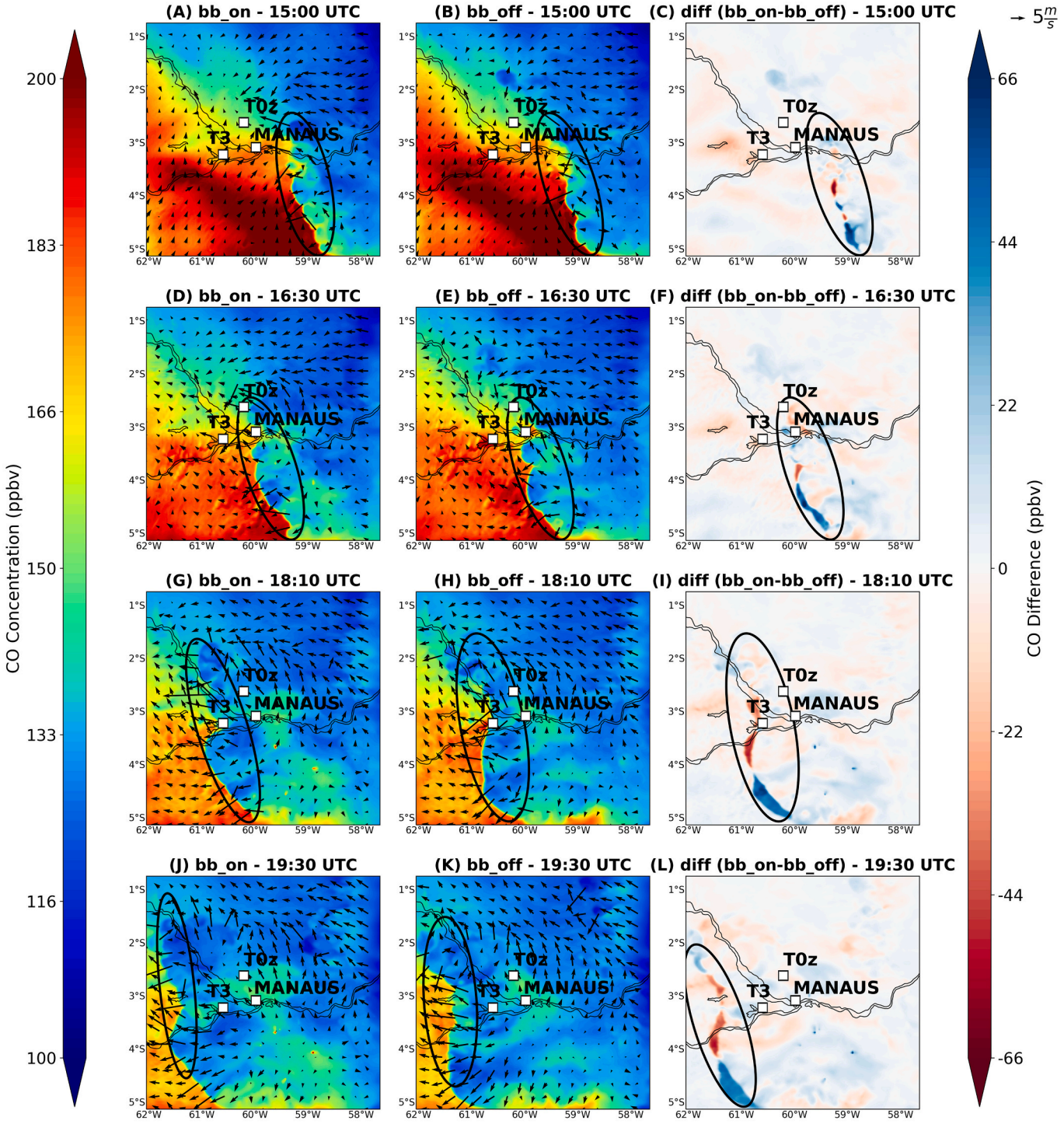

Fig. 13. Spatial distribution of surface-level CO concentration (ppbv) in the d03 domain at: 15 UTC on (A) bb_on; (B) bb_off; and (C) diff; at 16:30 UTC on (D) bb_on; (E) bb_off; and (F) diff; at 18:10 UTC on (G)bb_on; (H) bb_off; and (I) diff; at 19:30 UTC on (J) bb_on; (K) bb_off; and (L) diff.

$$fhO_3 = fU.fO_3 \quad (4)$$

$$fhCO = fU.fCO \quad (5)$$

It is possible to notice that during the downdraft occurrence at the T3 site, around 18:10 UTC, the simulations clearly show that there is a strong horizontal transport of O_3 and CO in the T3 site. Furthermore, the sign of the flux indicates the input (positive flux) or output (negative flux) of the scalar in the T3 region. The O_3 flux was positive, indicating the entry of O_3 into T3 during the presence of the MCS, corroborating with the results presented in Fig. 12. The CO fluxes were negative, indicating that the MCS removes them horizontally from the T3 site, similar to what was observed in Figs. 10 and 13. It is also clear from Fig. 14 that the horizontal fluxes during the downdraft were considerably higher for the bb_off simulation than for the bb_on simulation.

4. Conclusions

The WRF-Chem model was used to carry out simulations that allowed investigating how a scenario of increased fires in the Amazon

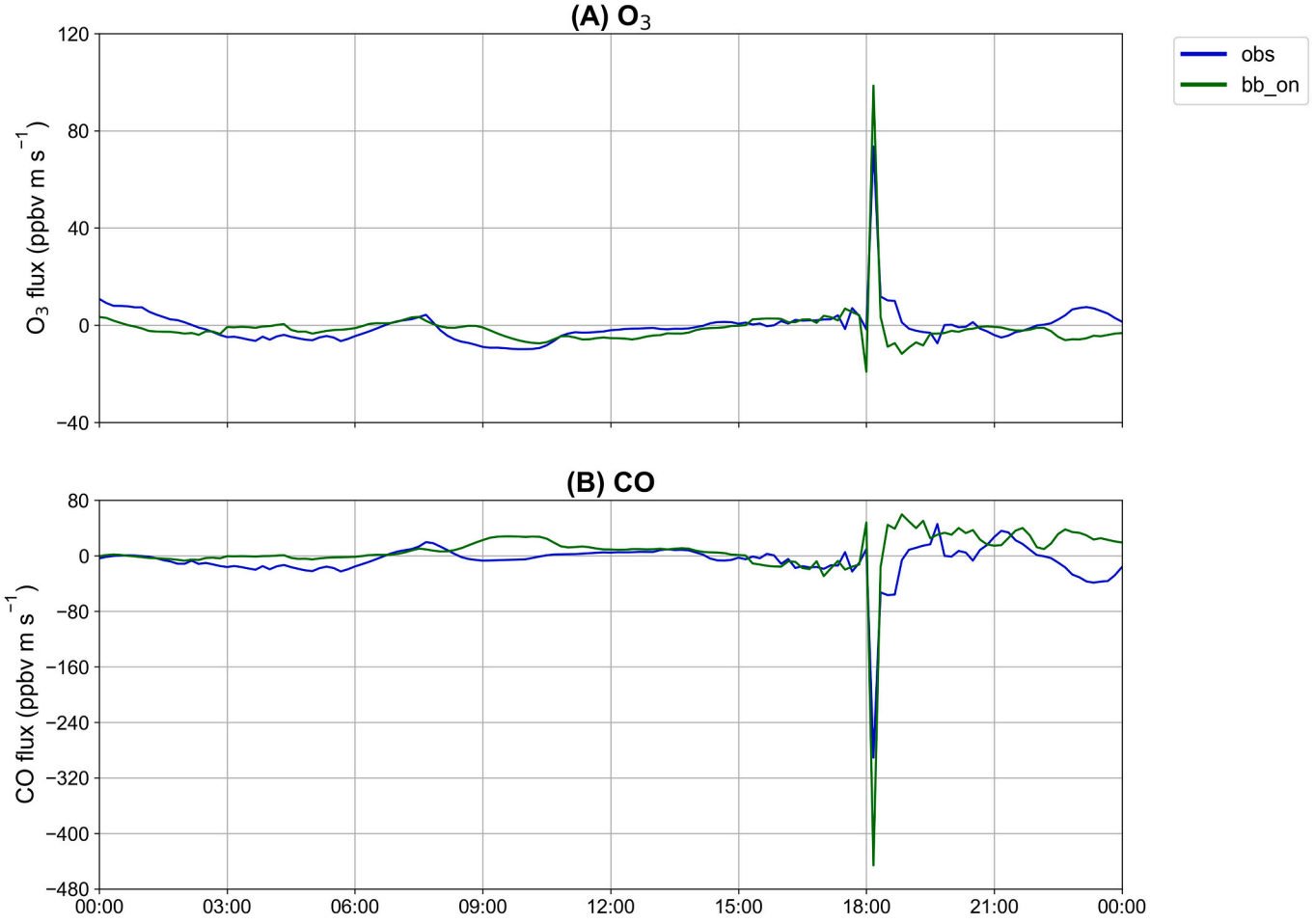

Fig. 14. Average horizontal fluxes at T3 of: (A) O_3 (ppbv m s^{-1}) and (B) CO (ppbv m s^{-1}).

region could influence deep convection and consequently the intensity of downdrafts, originating from MCS, in two different experimental sites located around of the City of Manaus, in the central Amazon. It is known that downdrafts can alter the thermodynamics and chemistry of the atmosphere near the surface. Thus, these simulations were performed for a case study of an MCS that passed through the central Amazon on August 16th, 2014. The two scenarios simulated were: 1) without the presence of fires (bb_off), and with the presence of fires (bb_on), where emissions from biomass burning were taken from FINN.

Both simulations satisfactorily reproduced the presence of downdrafts above the experimental sites, since: i) air temperature drops, ii) horizontal wind speed increases and iii) O_3 surface increases were reproduced by the simulations.

The presence of biomass burning aerosol in the simulation (bb_on) had important consequences on the formation of convective clouds and their downdrafts, that is, the convective clouds, located in the first 5 km, were less developed and were associated with lower rates of precipitation than for the bb_off simulation. Also for the bb_on simulations, the downdrafts were weaker (vertical wind speed less intense). Furthermore, the downdrafts simulated in the bb_on scenario were less efficient in reducing surface CO concentrations than the reduction observed in the bb_off simulation.

The simulations indicate that an increase in BB aerosol in the atmosphere can have important consequences on chemistry and thermodynamics near the surface, culminating in the intensity of storms.

In the present study it was also shown that in addition to vertical transport, downdrafts also play an important role in the horizontal transport of gases. The simulations carried out in this work showed that in an environment with greater fire emissions, downdrafts have a lower capacity to"clean up" the environment, that is, to dilute vertically and horizontally the local concentrations of gases such as CO.

Therefore, through the simulations carried out in this work, it was verified that the intensification of fires in the Amazon can lead to a scenario of clouds capable of producing lower precipitation rates and less efficient downdrafts in mixing the air layer located near the surface with the air above. This reduction in precipitation may further enhance the frequency of fire and associated aerosol emissions resulting in the potential for positive feedback that should be explored in future work.

Finally, we draw attention to the fact that trace gas and aerosol concentrations are sensitive to biomass burning emissions and to atmospheric transport including convective downdrafts. Convective processes are also sensitive to aerosol from biomass burning via both aerosol-cloud interactions and aerosol-radiation interactions. Ensemble simulations are required to help understand the relative sensitivity of trace gas and aerosol concentrations to emissions and atmospheric transport in this highly coupled system and to help identify the parameters and processes causing uncertainty in simulated concentrations.

CRediT authorship contribution statement

Flávio A.F. D'Oliveira: Conceptualization, Methodology, Writing – original draft, Writing – review & editing, Formal analysis. **Julia C.P. Cohen:** Conceptualization, Methodology, Writing – review & editing, Formal analysis. **Dominick V. Spracklen:** Methodology, Writing – review & editing. **Adan S.S. Medeiros:** Writing – review & editing.

Glauber G. Cirino: Writing – review & editing. **Paulo Artaxo:** Data curation. **Cleo Q. Dias-Júnior:** Conceptualization, Methodology, Writing – review & editing, Formal analysis.

Declaration of Competing Interest

The authors declare that they have no known competing financial interests or personal relationships that could have appeared to influence the work reported in this paper.

Acknowledgements

We acknowledge support from the Atmospheric Radiation Measurement (ARM) Climate Research Facility, a user facility of the United States Department of Energy (DOE) for the experimental T3 site data. Flávio A. F. D'Oliveira acknowledges CAPES (Coordenação de Aperfeiçoamento de Pessoal de Nível Superior) for the PhD scholarship and the support of a Royal Society Newton Advanced Fellowship (NAF\R1 \180405). This work was undertaken on ARC3, part of the High Performance Computing facilities at the University of Leeds, UK.

References

Ackerman, A.S., Toon, O.B., Stevens, D.E., Heymsfield, A.J., Ramanathan, V., Welton, E. J., 2000. Reduction of tropical cloudiness by soot. Science 288, 1042–1047. https://doi.org/10.1126/science.288.5468.1042.

Albrecht, B.A., 1989. Aerosols, cloud microphysics, and fractional cloudiness. Science 245, 1227–1230. https://doi.org/10.1126/science.245.4923.1227.

Andreae, M., Rosenfeld, D., 2008. Aerosol–cloud–precipitation interactions. Part 1. The nature and sources of cloud-active aerosols. Earth Sci. Rev. 89, 13–41. https://doi.org/10.1016/j.earscirev.2008.03.001.

Andreae, M.O., Rosenfeld, D., Artaxo, P., Costa, A.A., Frank, G.P., Longo, K.M., Silva-Dias, M.A.F., 2004. Smoking rain clouds over the amazon. Science 303, 1337–1342. https://doi.org/10.1126/science.1092779.

Araújo, A.C., 2002. Comparative measurements of carbon dioxide fluxes from two nearby towers in a central amazonian rainforest: the Manaus LBA site. J. Geophys. Res. 107 https://doi.org/10.1029/2001jd000676.

Archer-Nicholls, S., Lowe, D., Schultz, D.M., McFiggans, G., 2016. Aerosol–radiation–cloud interactions in a regional coupled model: the effects of convective parameterisation and resolution. Atmos. Chem. Phys. 16, 5573–5594. https://doi.org/10.5194/acp-16-5573-2016.

Barlow, J., Berenguer, E., Carmenta, R., França, F., 2019. Clarifying amazonia's burning crisis. Glob. Chang. Biol. 26, 319–321. https://doi.org/10.1111/gcb.14872.

Beck, V., Gerbig, C., Koch, T., Bela, M.M., Longo, K.M., Freitas, S.R., Kaplan, J.O., Prigent, C., Bergamaschi, P., Heimann, M., 2013. WRF-chem simulations in the amazon region during wet and dry season transitions: evaluation of methane models and wetland inundation maps. Atmos. Chem. Phys. 13, 7961–7982. https://doi.org/10.5194/acp-13-7961-2013.

Bela, M.M., Longo, K.M., Freitas, S.R., Moreira, D.S., Beck, V., Wofsy, S.C., Gerbig, C., Wiedemann, K., Andreae, M.O., Artaxo, P., 2015. Ozone production and transport over the amazon basin during the dry-to-wet and wet-to-dry transition seasons. Atmos. Chem. Phys. 15, 757–782. https://doi.org/10.5194/acp-15-757-2015.

Betts, A.K., 2002. Transport of ozone to the surface by convective downdrafts at night. J. Geophys. Res. 107 https://doi.org/10.1029/2000jd000158.

Bezerra, V.L., Dias-Júnior, C.Q., Vale, R.S., Santana, R.A., Botía, S., Manzi, A.O., Cohen, J.C.P., Martins, H.S., Chamecki, M., Fuentes, J.D., 2021. Near-surface atmospheric turbulence in the presence of a squall line above a forested and deforested region in the central amazon. Atmosphere 12, 461. https://doi.org/10.3390/atmos12040461.

Borge, R., Alexandrov, V., del Vas, J.J., Lumbreras, J., Rodríguez, E., 2008. A comprehensive sensitivity analysis of the WRF model for air quality applications over the iberian peninsula. Atmos. Environ. 42, 8560–8574. https://doi.org/10.1016/j.atmosenv.2008.08.032.

Butt, E.W., Conibear, L., Reddington, C.L., Darbyshire, E., Morgan, W.T., Coe, H., Artaxo, P., Brito, J., Knote, C., Spracklen, D.V., 2020. Large air quality and human health impacts due to amazon forest and vegetation fires. Environ. Res. Commun. 2, 095001. https://doi.org/10.1088/2515-7620/abb0db.

Butt, E.W., Conibear, L., Knote, C., Spracklen, D.V., 2021. Large air quality and public health impacts due to amazonian deforestation fires in 2019. Geohealth 5. https://doi.org/10.1029/2021gh000429.

Camponogara, G., Dias, M.A.F.S., Carrió, G.G., 2014. Relationship between amazon biomass burning aerosols and rainfall over the la Plata basin. Atmos. Chem. Phys. 14, 4397–4407. https://doi.org/10.5194/acp-14-4397-2014.

Charlson, R.J., Schwartz, S.E., Hales, J.M., Cess, R.D., Coakley, J.A., Hansen, J.E., Hofmann, D.J., 1992. Climate forcing by anthropogenic aerosols. Science 255, 423–430. https://doi.org/10.1126/science.255.5043.423.

Chate, D., Rao, P., Naik, M., Momin, G., Safai, P., Ali, K., 2003. Scavenging of aerosols and their chemical species by rain. Atmos. Environ. 37, 2477–2484. https://doi.org/10.1016/s1352-2310(03)00162-6.

Conibear, L., Butt, E.W., Knote, C., Arnold, S.R., Spracklen, D.V., 2018. Residential energy use emissions dominate health impacts from exposure to ambient particulate matter in india. Nat. Commun. 9 https://doi.org/10.1038/s41467-018-02986-7.

Dee, D.P., Uppala, S.M., Simmons, A.J., Berrisford, P., Poli, P., Kobayashi, S., Andrae, U., Balmaseda, M.A., Balsamo, G., Bauer, P., Bechtold, P., Beljaars, A.C.M., van de Berg, L., Bidlot, J., Bormann, N., Delsol, C., Dragani, R., Fuentes, M., Geer, A.J., Haimberger, L., Healy, S.B., Hersbach, H., Hólm, E.V., Isaksen, L., Kållberg, P., Köhler, M., Matricardi, M., McNally, A.P., Monge-Sanz, B.M., Morcrette, J.J., Park, B.K., Peubey, C., de Rosnay, P., Tavolato, C., Thépaut, J.N., Vitart, F., 2011. The ERA-interim reanalysis: configuration and performance of the data assimilation system. Q.J.R. Meteorol. Soc. 137, 553–597. https://doi.org/10.1002/qj.828.

Dentener, F., Kinne, S., Bond, T., Boucher, O., Cofala, J., Generoso, S., Ginoux, P., Gong, S., Hoelzemann, J., Ito, A., et al., 2006. Emissions of primary aerosol and precursor gases in the years 2000 and 1750 prescribed data-sets for aerocom. Atmos. Chem. Phys. 6, 4321–4344.

Dias, M.A.F.S., Dias, P.L.S., Longo, M., Fitzjarrald, D.R., Denning, A.S., 2004. River breeze circulation in eastern Amazonia: observations and modelling results. Theor. Appl. Climatol. 78 https://doi.org/10.1007/s00704–004–0047-6.

Dias-Júnior, C.Q., Sá, L.D., Filho, E.P.M., Santana, R.A., Mauder, M., Manzi, A.O., 2017. Turbulence regimes in the stable boundary layer above and within the amazon forest. Agric. For. Meteorol. 233, 122–132. https://doi.org/10.1016/j.agrformet.2016.11.001.

dos Santos, M.J., Dias, M.A.F.S., Freitas, E.D., 2014. Influence of local circulations on wind, moisture, and precipitation close to Manaus city, amazon region, Brazil. J. Geophys. Res. Atmos. 119, 13,233–13,249. https://doi.org/10.1002/2014jd021969.

Echalar, F.A.M., Artaxo, P., Martins, J.V., Yamasoe, M.A., Gerab, F., Maenhaut, W., Holben, B., 1998. Long-term monitoring of atmospheric aerosols in the amazon basin: source identification and apportionment. J. Geophys. Res. 103, 31849–31864. https://doi.org/10.1029/98jd01749.

Ek, M.B., Mitchell, K.E., Lin, Y., Rogers, E., Grunmann, P., Koren, V., Gayno, G., Tarpley, J.D., 2003. Implementation of noah land surface model advances in the national centers for environmental prediction operational mesoscale eta model. J. Geophys. Res. 108 https://doi.org/10.1029/2002jd003296.

ELETROBRÁS, 2014. Operation. https://eletrobras.com/en/Paginas/Operacao.aspx. Accessed 11.12.20.

Garstang, M., White, S., Shugart, H.H., Halverson, J., 1998. Convective cloud downdrafts as the cause of large blowdowns in the amazon rainforest. Meteorl. Atmos. Phys. 67, 199–212. https://doi.org/10.1007/bf01277510.

Gerken, T., Wei, D., Chase, R.J., Fuentes, J.D., Schumacher, C., Machado, L.A., Andreoli, R.V., Chamecki, M., de Souza, R.A.F., Freire, L.S., Jardine, A.B., Manzi, A. O., dos Santos, R.M.N., von Randow, C., dos Santos Costa, P., Stoy, P.C., Tóta, J., Trowbridge, A.M., 2016. Downward transport of ozone rich air and implications for atmospheric chemistry in the amazon rainforest. Atmos. Environ. 124, 64–76. https://doi.org/10.1016/j.atmosenv.2015.11.014.

Giangrande, S.E., Feng, Z., Jensen, M.P., Comstock, J.M., Johnson, K.L., Toto, T., Wang, M., Burleyson, C., Bharadwaj, N., Mei, F., Machado, L.A.T., Manzi, A.O., Xie, S., Tang, S., Dias, M.A.F.S., de Souza, R.A.F., Schumacher, C., Martin, S.T., 2017. Cloud characteristics, thermodynamic controls and radiative impacts during the observations and modeling of the green ocean amazon (GoAmazon2014/5) experiment. Atmos. Chem. Phys. 17, 14519–14541. https://doi.org/10.5194/acp-17-14519-2017.

Giglio, L., 2007. Characterization of the tropical diurnal fire cycle using virs and modis observations. Remote Sens. Environ. 108, 407–421.

Giglio, L., Descloitres, J., Justice, C.O., Kaufman, Y.J., 2003. An enhanced contextual fire detection algorithm for MODIS. Remote Sens. Environ. 87, 273–282. https://doi.org/10.1016/s0034-4257(03)00184-6.

Gonçalves, W.A., Machado, L.A.T., Kirstetter, P.E., 2015. Influence of biomass aerosol on precipitation over the central amazon: an observational study. Atmos. Chem. Phys. 15, 6789–6800. https://doi.org/10.5194/acp-15-6789-2015.

Gonzalez-Alonso, L., Val Martin, M., Kahn, R.A., 2019. Biomass-burning smoke heights over the amazon observed from space. Atmos. Chem. Phys. 19, 1685–1702.

Grell, G.A., Peckham, S.E., Schmitz, R., McKeen, S.A., Frost, G., Skamarock, W.C., Eder, B., 2005. Fully coupled "online" chemistry within the WRF model. Atmos. Environ. 39, 6957–6975. https://doi.org/10.1016/j.atmosenv.2005.04.027.

Hersbach, H., Bell, B., Berrisford, P., Hirahara, S., Horányi, A., Muñoz-Sabater, J., Nicolas, J., Peubey, C., Radu, R., Schepers, D., Simmons, A., Soci, C., Abdalla, S., Abellan, X., Balsamo, G., Bechtold, P., Biavati, G., Bidlot, J., Bonavita, M., Chiara, G., Dahlgren, P., Dee, D., Diamantakis, M., Dragani, R., Flemming, J., Forbes, R., Fuentes, M., Geer, A., Haimberger, L., Healy, S., Hogan, R.J., Hólm, E., Janisková, M., Keeley, S., Laloyaux, P., Lopez, P., Lupu, C., Radnoti, G., Rosnay, P., Rozum, I., Vamborg, F., Villaume, S., Thépaut, J.N., 2020. The ERA5 global reanalysis. Q.J.R. Meteorol. Soc. 146, 1999–2049. https://doi.org/10.1002/qj.3803.

Hodzic, A., Knote, C., 2014. Mozart gas-phase chemistry with mosaic aerosols. In: NCAR/ACD. Readme Document.

Houze, R.A., 2004. Mesoscale convective systems. Rev. Geophys. 42 https://doi.org/10.1029/2004rg000150.

Iacono, M.J., Delamere, J.S., Mlawer, E.J., Shephard, M.W., Clough, S.A., Collins, W.D., 2008. Radiative forcing by long-lived greenhouse gases: calculations with the AER radiative transfer models. J. Geophys. Res. 113 https://doi.org/10.1029/2008jd009944.

Ibarra-Espinosa, S., Ynoue, R., O'Sullivan, S., Pebesma, E., de Fátima Andrade, M., Osses, M., 2018. VEIN v0.2.2: an r package for bottom–up vehicular emissions inventories. Geosci. Model Dev. 11, 2209–2229. https://doi.org/10.5194/gmd-11-2209-2018.

Janssens-Maenhout, G., Crippa, M., Guizzardi, D., Muntean, M., Schaaf, E., Dentener, F., Bergamaschi, P., Pagliari, V., Olivier, J.G.J., Peters, J.A.H.W., van Aardenne, J.A., Monni, S., Doering, U., Petrescu, A.M.R., Solazzo, E., Oreggioni, G.D., 2019. EDGAR v4.3.2 global atlas of the three major greenhouse gas emissions for the period 1970–2012. Earth Syst. Sci. Data 11, 959–1002. https://doi.org/10.5194/essd-11-959-2019.

Jiang, H., Feingold, G., 2006. Effect of aerosol on warm convective clouds: aerosol-cloud-surface flux feedbacks in a new coupled large eddy model. J. Geophys. Res. 111 https://doi.org/10.1029/2005jd006138.

Junior, C.H.L.S., Pessôa, A.C.M., Carvalho, N.S., Reis, J.B.C., Anderson, L.O., Aragão, L.E. O.C., 2020. The brazilian amazon deforestation rate in 2020 is the greatest of the decade. Nat. Ecol. Evol. Evol. 5, 144–145. https://doi.org/10.1038/s41559-020-01368-x.

Kaufman, Y.J., Koren, I., 2006. Smoke and pollution aerosol effect on cloud cover. Science 313, 655–658. https://doi.org/10.1126/science.1126232.

Knote, C., Hodzic, A., Jimenez, J.L., Volkamer, R., Orlando, J.J., Baidar, S., Brioude, J., Fast, J., Gentner, D.R., Goldstein, A.H., Hayes, P.L., Knighton, W.B., Oetjen, H., Setyan, A., Stark, H., Thalman, R., Tyndall, G., Washenfelder, R., Waxman, E., Zhang, Q., 2014. Simulation of semi-explicit mechanisms of SOA formation from glyoxal in aerosol in a 3-d model. Atmos. Chem. Phys. 14, 6213–6239. https://doi.org/10.5194/acp-14-6213-2014.

Knote, C., Hodzic, A., Jimenez, J.L., 2015. The effect of dry and wet deposition of condensable vapors on secondary organic aerosols concentrations over the continental US. Atmos. Chem. Phys. 15, 1–18. https://doi.org/10.5194/acp-15-1-2015.

Kolusu, S.R., Marsham, J.H., Mulcahy, J., Johnson, B., Dunning, C., Bush, M., Spracklen, D.V., 2015. Impacts of Amazonia biomass burning aerosols assessed from short-range weather forecasts. Atmos. Chem. Phys. 15, 12251–12266. https://doi.org/10.5194/acp-15-12251-2015.

Koren, I., Kaufman, Y.J., Remer, L.A., Martins, J.V., 2004. Measurement of the effect of amazon smoke on inhibition of cloud formation. Science 303, 1342–1345. https://doi.org/10.1126/science.1089424.

Koren, I., Martins, J.V., Remer, L.A., Afargan, H., 2008. Smoke invigoration versus inhibition of clouds over the amazon. Science 321, 946–949. https://doi.org/10.1126/science.1159185.

Lamarque, J.F., Emmons, L.K., Hess, P.G., Kinnison, D.E., Tilmes, S., Vitt, F., Heald, C.L., Holland, E.A., Lauritzen, P.H., Neu, J., Orlando, J.J., Rasch, P.J., Tyndall, G.K., 2012. CAM-chem: description and evaluation of interactive atmospheric chemistry in the community earth system model. Geosci. Model Dev. 5, 369–411. https://doi.org/10.5194/gmd-5-369-2012.

Lin, J.C., Matsui, T., Pielke, R.A., Kummerow, C., 2006. Effects of biomass-burning-derived aerosols on precipitation and clouds in the amazon basin: a satellite-based empirical study. J. Geophys. Res. 111 https://doi.org/10.1029/2005jd006884.

Liu, L., Cheng, Y., Wang, S., Wei, C., Pöhlker, M., Pöhlker, C., Artaxo, P., Shrivastava, M., Andreae, M.O., Pöschl, U., Su, H., 2020. Impact of Biomass Burning Aerosols on Radiation, Clouds, and Precipitation over the Amazon during the Dry Season: Dependence of Aerosol-Cloud and Aerosol-Radiation Interactions on Aerosol Loading. https://doi.org/10.5194/acp-2020-191.

Machado, L.A.T., Calheiros, A.J.P., Biscaro, T., Giangrande, S., Dias, M.A.F.S., Cecchini, M.A., Albrecht, R., Andreae, M.O., Araujo, W.F., Artaxo, P., Borrmann, S., Braga, R., Burleyson, C., Eichholz, C.W., Fan, J., Feng, Z., Fisch, G.F., Jensen, M.P., Martin, S.T., Pöschl, U., Pöhlker, C., Pöhlker, M.L., Ribaud, J.F., Rosenfeld, D., Saraiva, J.M.B., Schumacher, C., Thalman, R., Walter, D., Wendisch, M., 2018. Overview: precipitation characteristics and sensitivities to environmental conditions during GoAmazon2014/5 and ACRIDICON-CHUVA. Atmos. Chem. Phys. 18, 6461–6482. https://doi.org/10.5194/acp-18-6461-2018.

Marenco, F., Johnson, B., Langridge, J.M., Mulcahy, J., Benedetti, A., Remy, S., Jones, L., Szpek, K., Haywood, J., Longo, K., et al., 2016. On the vertical distribution of smoke in the amazonian atmosphere during the dry season. Atmos. Chem. Phys. 16, 2155–2174.

Marengo, J.A., Liebmann, B., Kousky, V.E., Filizola, N.P., Wainer, I.C., 2001. Onset and end of the rainy season in the brazilian amazon basin. J. Clim. 14, 833–852. https://doi.org/10.1175/1520-0442(2001)014<0833:oaeotr>2.0.co;2.

Marinho, R.R., Junior, N.P.F., Cremon, É.H., 2020. Analysis of suspended sediment in the anavilhanas archipelago, Rio Negro, amazon basin. Water 12, 1073. https://doi.org/10.3390/w12041073.

Martin, S.T., Andreae, M.O., Artaxo, P., Baumgardner, D., Chen, Q., Goldstein, A.H., Guenther, A., Heald, C.L., Mayol-Bracero, O.L., McMurry, P.H., Pauliquevis, T., Pöschl, U., Prather, K.A., Roberts, G.C., Saleska, S.R., Dias, M.A.S., Spracklen, D.V., Swietlicki, E., Trebs, I., 2010. Sources and properties of amazonian aerosol particles. Rev. Geophys. 48 https://doi.org/10.1029/2008rg000280.

Martin, S.T., Artaxo, P., Machado, L.A.T., Manzi, A.O., Souza, R.A.F., Schumacher, C., Wang, J., Andreae, M.O., Barbosa, H.M.J., Fan, J., Fisch, G., Goldstein, A.H., Guenther, A., Jimenez, J.L., Pöschl, U., Dias, M.A.S., Smith, J.N., Wendisch, M., 2016. Introduction: Observations and modeling of the green ocean amazon (GoAmazon2014/5). Atmos. Chem. Phys. 16, 4785–4797. https://doi.org/10.5194/acp-16-4785-2016.

Martins, J.A., Dias, M.A.F.S., Gonçalves, F.L.T., 2009. Impact of biomass burning aerosols on precipitation in the amazon: a modeling case study. J. Geophys. Res. 114 https://doi.org/10.1029/2007jd009587.

Medeiros, A.S.S., Calderaro, G., Guimarães, P.C., Magalhaes, M.R., Morais, M.V.B., Rafee, S.A.A., Ribeiro, I.O., Andreoli, R.V., Martins, J.A., Martins, L.D., Martin, S.T., Souza, R.A.F., 2017. Power plant fuel switching and air quality in a tropical, forested environment. Atmos. Chem. Phys. 17, 8987–8998. https://doi.org/10.5194/acp-17-8987-2017.

Melo, A.M., Dias-Junior, C.Q., Cohen, J.C., Sá, L.D., Cattanio, J.H., Kuhn, P.A., 2019. Ozone transport and thermodynamics during the passage of squall line in central amazon. Atmos. Environ. 206, 132–143. https://doi.org/10.1016/j.atmosenv.2019.02.018.

Mendonça, A.C.S.D., 2021. Regimes de turbulência na camada limite atmosférica: interação com a convecção profunda e a mortalidade de árvores na Amazônia. Master's thesis. Instituto Nacional de Pesquisas da Amazônia-INPA, Manaus, Brazil.

Morrison, H., Thompson, G., Tatarskii, V., 2009. Impact of cloud microphysics on the development of trailing stratiform precipitation in a simulated squall line: comparison of one- and two-moment schemes. Mon. Weather Rev. 137, 991–1007. https://doi.org/10.1175/2008mwr2556.1.

Nakanishi, M., Niino, H., 2009. Development of an improved turbulence closure model for the atmospheric boundary layer. J. Meteorol. Soc. Jpn. 87, 895–912. https://doi.org/10.2151/jmsj.87.895.

Nascimento, J.P., Bela, M.M., Meller, B.B., Banducci, A.L., Rizzo, L.V., Vara-Vela, A.L., Barbosa, H.M.J., Gomes, H., Rafee, S.A.A., Franco, M.A., Carbone, S., Cirino, G.G., Souza, R.A.F., McKeen, S.A., Artaxo, P., 2021. Aerosols from anthropogenic and biogenic sources and their interactions – modeling aerosol formation, optical properties, and impacts over the central amazon basin. Atmos. Chem. Phys. 21, 6755–6779. https://doi.org/10.5194/acp-21-6755-2021.

Rafee, S.A.A., Martins, L.D., Kawashima, A.B., Almeida, D.S., Morais, M.V.B., Souza, R.V. A., Oliveira, M.B.L., Souza, R.A.F., Medeiros, A.S.S., Urbina, V., Freitas, E.D., Martin, S.T., Martins, J.A., 2017. Contributions of mobile, stationary and biogenic sources to air pollution in the amazon rainforest: a numerical study with the WRF-chem model. Atmos. Chem. Phys. 17, 7977–7995. https://doi.org/10.5194/acp-17-7977-2017.

Ramanathan, V., Crutzen, P.J., Kiehl, J.T., Rosenfeld, D., 2001. Aerosols, climate, and the hydrological cycle. Science 294, 2119–2124. https://doi.org/10.1126/science.1064034.

Reddington, C.L., Butt, E.W., Ridley, D.A., Artaxo, P., Morgan, W.T., Coe, H., Spracklen, D.V., 2015. Air quality and human health improvements from reductions in deforestation-related fire in Brazil. Nat. Geosci. 8, 768–771. https://doi.org/10.1038/ngeo2535.

Rehbein, A., Ambrizzi, T., Mechoso, C.R., 2017. Mesoscale convective systems over the amazon basin. Part i: climatological aspects. Int. J. Climatol. 38, 215–229. https://doi.org/10.1002/joc.5171.

Rehbein, A., Ambrizzi, T., Mechoso, C.R., Espinosa, S.A.I., Myers, T.A., 2019. Mesoscale convective systems over the amazon basin: the GoAmazon2014/5 program. Int. J. Climatol. 39, 5599–5618. https://doi.org/10.1002/joc.6173.

Rissler, J., Swietlicki, E., Zhou, J., Roberts, G., Andreae, M.O., Gatti, L.V., Artaxo, P., 2004. Physical properties of the sub-micrometer aerosol over the amazon rain forest during the wet-to-dry season transition - comparison of modeled and measured CCN concentrations. Atmos. Chem. Phys. 4, 2119–2143. https://doi.org/10.5194/acp-4-2119-2004.

Rizzo, L.V., Artaxo, P., Müller, T., Wiedensohler, A., Paixão, M., Cirino, G.G., Arana, A., Swietlicki, E., Roldin, P., Fors, E.O., Wiedemann, K.T., Leal, L.S.M., Kulmala, M., 2013. Long term measurements of aerosol optical properties at a primary forest site in Amazonia. Atmos. Chem. Phys. 13, 2391–2413. https://doi.org/10.5194/acp-13-2391-2013.

Roberts, G.C., 2003. Impact of biomass burning on cloud properties in the amazon basin. J. Geophys. Res. 108 https://doi.org/10.1029/2001jd000985.

Roberts, G.C., Andreae, M.O., Zhou, J., Artaxo, P., 2001. Cloud condensation nuclei in the amazon basin: "marine" conditions over a continent? Geophys. Res. Lett. 28, 2807–2810. https://doi.org/10.1029/2000gl012585.

Rosenfeld, D., 1999. TRMM observed first direct evidence of smoke from forest fires inhibiting rainfall. Geophys. Res. Lett. 26, 3105–3108. https://doi.org/10.1029/1999gl006066.

Rosenfeld, D., Lohmann, U., Raga, G.B., O'Dowd, C.D., Kulmala, M., Fuzzi, S., Reissell, A., Andreae, M.O., 2008. Flood or drought: how do aerosols affect precipitation? Science 321, 1309–1313. https://doi.org/10.1126/science.1160606.

Santana, R.A., Dias-Júnior, C.Q., da Silva, J.T., Fuentes, J.D., do Vale, R.S., Alves, E.G., dos Santos, R.M.N., Manzi, A.O., 2018. Air turbulence characteristics at multiple sites in and above the amazon rainforest canopy. Agric. For. Meteorol. 260-261, 41–54. https://doi.org/10.1016/j.agrformet.2018.05.027.

Scala, J.R., Garstang, M., Kuo Tao, W., Pickering, K.E., Thompson, A.M., Simpson, J., Kirchhoff, V.W.J.H., Browell, E.V., Sachse, G.W., Torres, A.L., Gregory, G.L., Rasmussen, R.A., Khalil, M.A.K., 1990. Cloud draft structure and trace gas transport. J. Geophys. Res. 95, 17015. https://doi.org/10.1029/jd095id10p17015.

Schwartz, S.E., Buseck, P.R., 2000. Absorbing phenomena. Science 288, 989–990. https://doi.org/10.1126/science.288.5468.989.

Silver, B., Conibear, L., Reddington, C.L., Knote, C., Arnold, S.R., Spracklen, D.V., 2020. Pollutant emission reductions deliver decreased $pm_{2.5}$ -caused mortality across China during 2015-2017. Atmos. Chem. Phys. 20, 11683–11695. https://doi.org/10.5194/acp-20-11683-2020.

Spracklen, D.V., Carslaw, K.S., Pöschl, U., Rap, A., Forster, P.M., 2011. Global cloud condensation nuclei influenced by carbonaceous combustion aerosol. Atmos. Chem. Phys. 11, 9067–9087. https://doi.org/10.5194/acp-11-9067-2011.

Tao, W.K., Chen, J.P., Li, Z., Wang, C., Zhang, C., 2012. Impact of aerosols on convective clouds and precipitation. Rev. Geophys. 50 https://doi.org/10.1029/2011rg000369.

Tie, X., 2003. Effect of clouds on photolysis and oxidants in the troposphere. J. Geophys. Res. 108 https://doi.org/10.1029/2003jd003659.

Trebs, I., Mayol-Bracero, O.L., Pauliquevis, T., Kuhn, U., Sander, R., Ganzeveld, L., Meixner, F.X., Kesselmeier, J., Artaxo, P., Andreae, M.O., 2012. Impact of the Manaus urban plume on trace gas mixing ratios near the surface in the amazon basin: Implications for the NO-NO2-o3photostationary state and peroxy radical levels. J. Geophys. Res. 117 https://doi.org/10.1029/2011jd016386 n/a–n/a.

Vestin, A., Rissler, J., Swietlicki, E., Frank, G.P., Andreae, M.O., 2007. Cloud-nucleating properties of the amazonian biomass burning aerosol: Cloud condensation nuclei measurements and modeling. J. Geophys. Res. 112 https://doi.org/10.1029/2006jd008104.

Wiedinmyer, C., Akagi, S.K., Yokelson, R.J., Emmons, L.K., Al-Saadi, J.A., Orlando, J.J., Soja, A.J., 2011. The fire INventory from NCAR (FINN): a high resolution global model to estimate the emissions from open burning. Geosci. Model Dev. 4, 625–641. https://doi.org/10.5194/gmd-4-625-2011.

Williams, E., 2002. Contrasting convective regimes over the amazon: implications for cloud electrification. J. Geophys. Res. 107 https://doi.org/10.1029/2001jd000380.

Wu, L., Su, H., Jiang, J.H., 2011. Regional simulations of deep convection and biomass burning over south america: 2. Biomass burning aerosol effects on clouds and precipitation. J. Geophys. Res. 116 https://doi.org/10.1029/2011jd016106.

Zaveri, R.A., Easter, R.C., Fast, J.D., Peters, L.K., 2008. Model for simulating aerosol interactions and chemistry (MOSAIC). J. Geophys. Res. 113 https://doi.org/10.1029/2007jd008782.